Query Details

Back to Main Page

1. Kindly check and confirm the given name and family name are correct for authors (Siamak Nikzad Khangholi, X. Grant Chen).

2. Kindly provide a complete detail for reference (Martinova 2003).

Review

Review on recent progress in Al–Mg–Si 6xxx conductor alloys

Siamak Nikzad Khangholi Affiliationids : Aff1

Mousa Javidani ✉

Email : mousa_javidani@uqac.ca

Affiliationids : Aff1, Correspondingaffiliationid : Aff1

Alexandre Maltais Affiliationids : Aff2

X. Grant Chen Affiliationids : Aff1

Aff1 Department of Applied Science, University of Québec at Chicoutimi, Saguenay, QC, G7H 2B1, Canada

Aff2 Arvida Research and Development Center, Rio Tinto Aluminum, Saguenay, QC, G7S 4K8, Canada

Received: 21 October 2021 / Accepted: 4 January 2022

Abstract

AQ1 The mechanical strength and electrical conductivity (EC) in Al–Mg–Si 6xxx conductor alloys are key characteristics but mutually exclusive properties. This review paper critically elaborates the methods to enhance the mechanical strength and electrical conductivity. These methods include an optimization of the main alloying elements (Mg and Si), the addition of the other alloying elements, melt treatment, applying the modified thermomechanical treatments, and maximizing the area reduction (severe plastic deformation) in the wire drawing. Besides, the impact of the various microstructural features on the mechanical and electrical properties is addressed in detail using strength and electrical resistivity models. A principal conclusion drawn in this review is that the strength ought to be enhanced by creating barriers (such as sessile dislocations and precipitates) for dislocation movement while having a less detrimental effect on the electrical conductivity. Considering the potential of Al–Mg–Si conductor alloys, future directions are outlined.

Graphical abstract

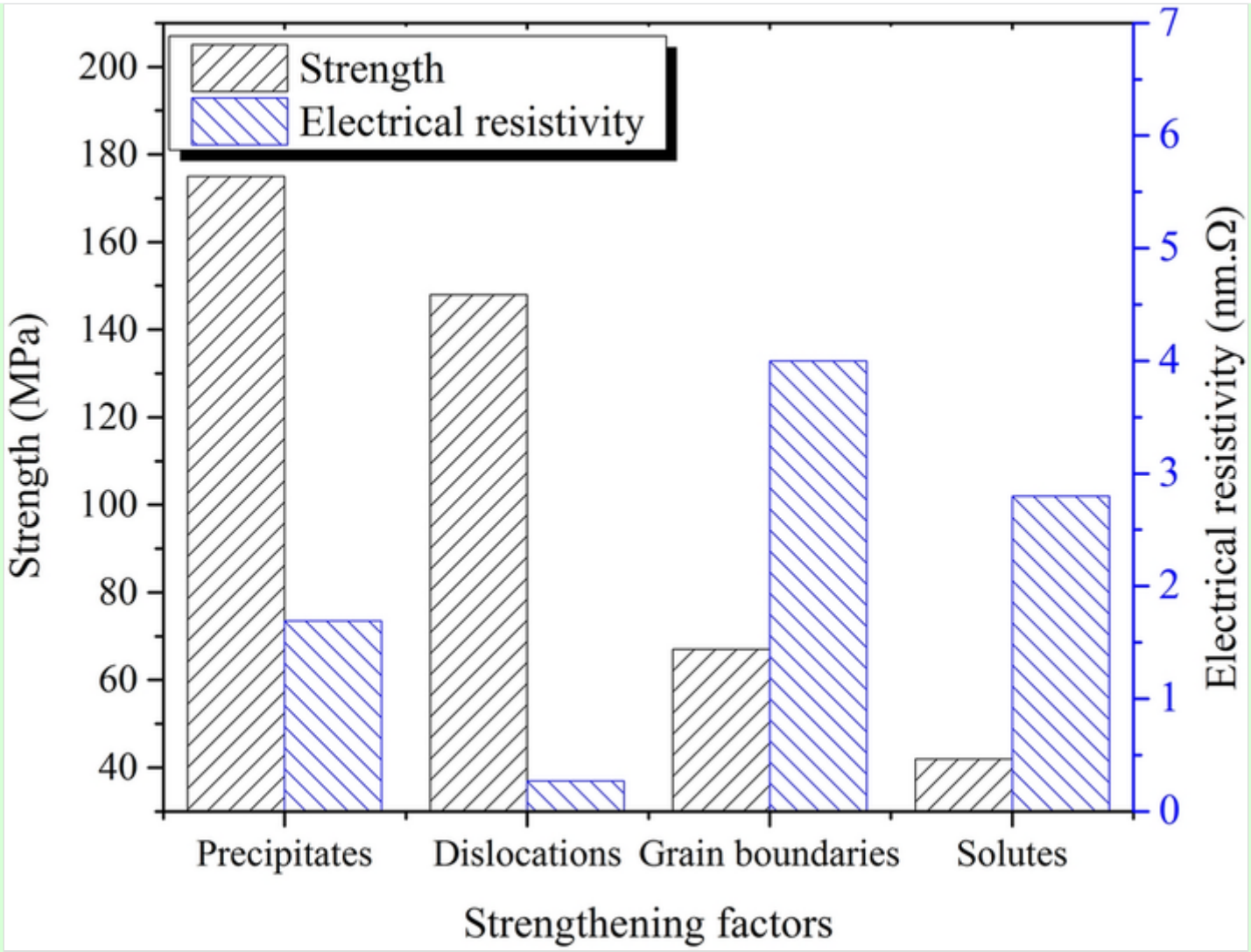

Keywords

Al–Mg–Si conductor alloys
Mechanical properties
Electrical conductivity
Alloying elements
Thermomechanical treatment
Strength and electrical resistivity models

Supplementary Information

The online version contains supplementary material available at https://doi.org/10.1557/s43578-022-00488-3.

Introduction

Owing to the ever-increasing demands, developing high strength and highly conductive cables has received great attention in research in recent decades. Aluminum alloys have been considered an appropriate substitution for copper conductors owing to their distinctive properties, such as lower cost and higher strength/weight ratio, relative to Cu conductors [1, 2, 3]. Conductors made of aluminum alloys present inferior electrical conductivity (EC), but their density is one-third that of Cu conductors. The mass resistivity is defined by the combination of the electrical resistivity and density. Therefore, the high mass resistivity of Cu conductors, which is approximately twice as high as that of aluminum conductors, implies a relatively higher conduction capacity in Al conductors than in Cu conductors with the same weight [2].

Aluminum conductors are categorized into two main groups for overhead power lines: aluminum conductor steel reinforced (ACSR) and all-aluminum alloy conductor (AAAC) (Supplementary Fig. S1). ACSR is composed of steel in the core surrounded by high conductivity pure aluminum (such as AA1350) [4, 5, 6, 7, 8]. Due to the low strength of pure Al alloys, ACSR is reinforced by the steel core to sustain a large stress [4]. To respect the high corrosion resistance and mechanical property requirements in high-voltage transmission lines, AAAC has been introduced as an alternative for ACSR in recent years, which are self-supporting overhead power lines. Among aluminum alloys, 6xxx series (Al–Mg–Si) conductor alloys are known as materials used in AAAC owing to their high strength via the aging process with a desirable EC. Another type of aluminum conductor is aluminum conductor alloy reinforced (ACAR). This conductor is a concentric-lay stranded conductor made up of AA 1350 and AA 6201 strands. The AA6201 alloy is in the core of the conductor (the AA 1350 strands) to reinforce them [5, 6, 7, 9]. Despite the relatively high corrosion resistance of 6xxx series alloys, their corrosion resistance has also been taken into account for further improvement in some research works [10, 11].

In general, there is a compromise between strength and EC in aluminum alloys, as shown in Fig. 1 [12]. However, two well-known AA6101 and AA6201 alloys that serve as conductors in AAAC show a better trade-off between strength and EC among 6xxx series conductor alloys [5, 6, 12, 13]. Overall, the AA6201 alloy possesses higher Mg and Si than the AA6101 alloy, yielding a higher strength and lower EC than the AA6101 alloy [5, 6]. Based on Fig. 1, the dotted line shows the upper limit for commercial aluminum alloys in terms of the combination between strength and EC. Therefore, the achievement of strength and EC above the dotted line is technically a challenging issue [12].

Figure 1

Plot of strength versus EC for several commercial aluminum alloys [12].

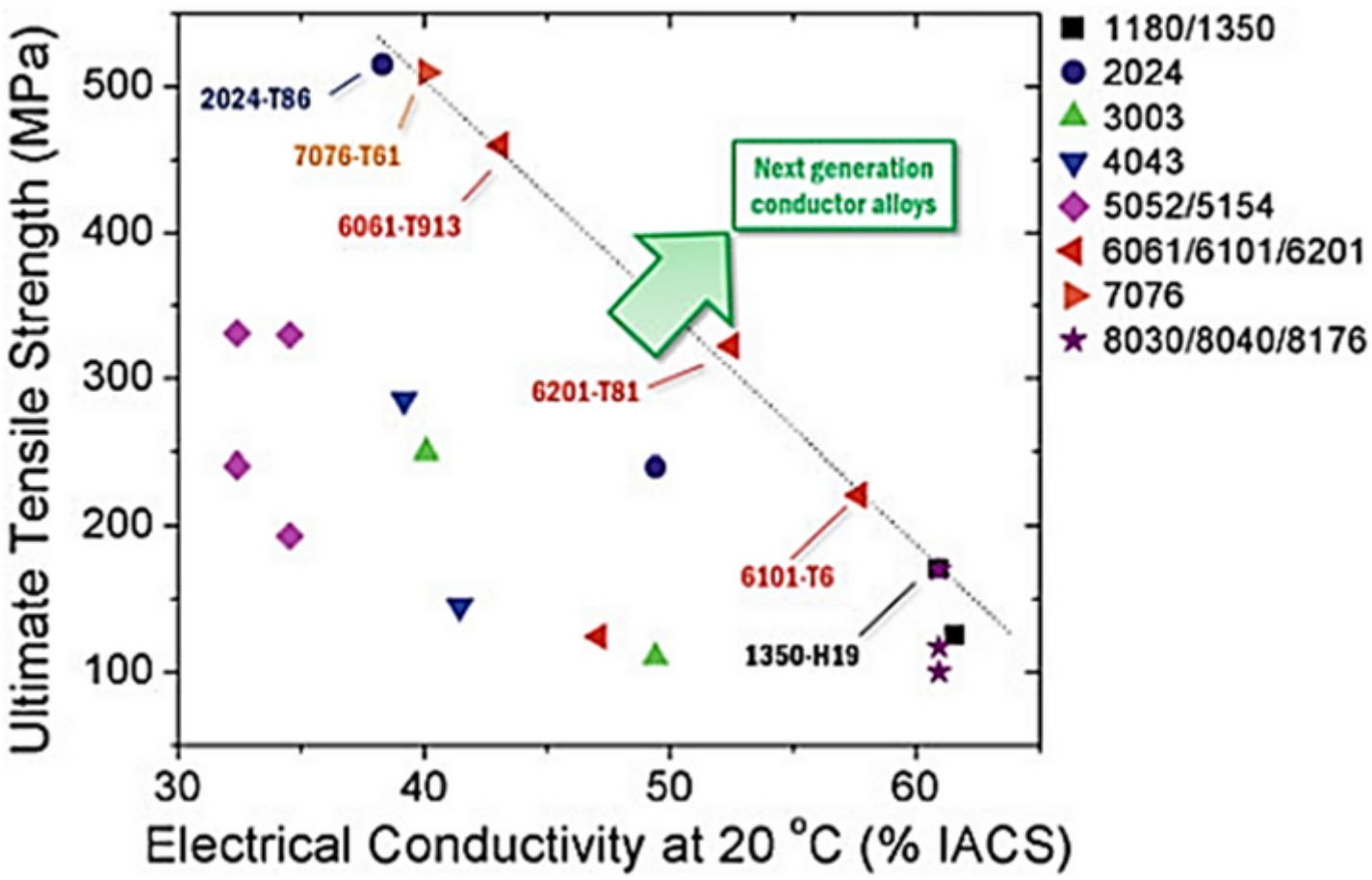

The principal strengthening mechanisms of aluminum alloys are precipitation hardening, work hardening, solute strengthening, and grain boundary strengthening. On the other hand, the EC of metals is correlated with the behavior of valence electrons. Similarly, the cause of electrical resistivity is the disruption of the atomic periodicity in a crystal structure, resulting from crystal defects (e.g., vacancies, dislocations, and grain boundaries), precipitates, and impurity atoms in a pure metal lattice [14, 15, 16, 17]. Among these parameters, impurity atoms in the matrix along with Guinier–Preston (GP) zones possess the most detrimental effects on EC. In general, the resistivity impact of the solutes is much stronger than GP zones [15, 16, 18]. Consequently, it could be inferred that the parameters resulting in an improvement in strength give rise to higher electrical resistivity, meaning that EC and strength are mutually exclusive [14, 15, 16, 19]. The minimum required EC and strength for Al–Mg–Si conductor alloys are provided in the EN 50183, ASTM B398, and ASTM B317 standards. In general, the minimum EC of the Al–Mg–Si conductor alloys is required to be 52.5% IACS (See Supplementary Table S1) [20, 21, 22].

Aside from the EC and mechanical properties of all-aluminum alloy conductors, their fatigue life and failure analysis have been investigated recently [4, 23]. It is well understood that the loads caused by the conductor weight, wind, and ice are among the main forces, ending up to conductor damage. The applied forces could cause the bending of cable strands, subsequently leading to friction between the conductor and the suspension clamp known as fretting fatigue/wear phenomena [4, 23]. The service life of the conductors is planned to be ~ 30 years.

The main scope of this paper is to address the strength and EC improvement in Al–Mg–Si conductor alloys. Although significant efforts have been directed toward a simultaneous enhancement of electrical and mechanical properties in Al–Mg–Si conductor alloys, the correlation between strength/EC and microstructure is still debatable in terms of the different variables influencing chemical composition and thermomechanical treatment. The present study aims to discuss and critically review the effects of various parameters on the improvement of electrical and mechanical properties of 6xxx series conductor alloys.

In general, a better combination of strength and EC in 6xxx series conductor cables could be obtained through:

1. Chemical compositions
   a. Optimal levels of the principal alloying elements [15, 24, 25, 26, 27].
   b. Desirable amounts of additional alloying elements [12, 28].
   c. Grain refiners and modifiers [5, 29].
2. Thermomechanical processes
   a. Conventional/modified thermomechanical treatment [12, 19, 30, 31, 32].
   b. Severe plastic deformation [16, 18, 33, 34, 35].

Fabrication processes of 6xxx electrical conductors

In the upcoming sections, the effect of the various parameters during the fabrication process on the strength and EC will be discussed. Thus, it is worthwhile to identify the stages of different fabrication processes.

Over the last decades, two distinct fabrication processes have been developed to produce redraw rods: (a) direct chill (DC) casting followed by an extrusion process and (b) continuous casting followed by a hot rolling process [6, 36]. In the former case, the prepared molten metal

in the furnace is inoculated (e.g., by Al-B master alloy) while being transferred to the cast mold through a tundish. The DC-cast billets are subsequently hot-extruded into 9.5 mm rods after being homogenized (such as at 560 °C for 6 h) [6].

The predominant fabrication process of the redraw rods is by means of Properzi continuous casting followed by a hot rolling process (Fig. 2) [37]. In the process, once the target chemical composition is achieved, the molten metal is further treated inside the furnace by adding an appropriate grain refiner and modifier (such as Al-Ti-B and Al-B master alloys). Subsequently, the molten metal is transferred via a tundish and poured into a grooved wheel mold made of copper (Fig. 2 a). The mold, which is partially surrounded by a steel belt, is exposed to water spray cooling to ensure desirable solidification conditions [6, 38, 39, 40]. This casting technique, which is called Properzi caster, produces cast bars with a trapezoidal cross section. The cast bar is subsequently directed to an in-line multiple hot rolling process unit, through which the trapezoidal cross section of the bar is transformed into a circular rod with a diameter of 9.5 mm (Fig. 2 b) [6, 39]. The temperature of the cast bar before hot rolling is carefully controlled to keep the alloys above the solvus temperature to ensure the supersaturated solid solution. The rolled aluminum rod is finally packaged as a coil of several tons [38]. Afterward, the coils are transported to a downstream fabricator of wire drawing (Fig. 2 c), through which the rods are drawn to wires with desired diameters ($ø$ = 1.5–5.0 mm). The drawn wires are subsequently subjected to artificial aging treatment to improve the strength and EC (Fig. 2 d) [6, 39]. Other manufacturing techniques, such as horizontal continuous casting and semisolid continuous casting followed by an extrusion process, can also be employed to produce aluminum wire rods [36, 41]; however, these techniques may not be as commercially viable as the first two aforementioned techniques.

Figure 2

Production chain of Properzi process followed by wire drawing and aging treatment for aluminum conductive cables

Reprinted with permission from [37].

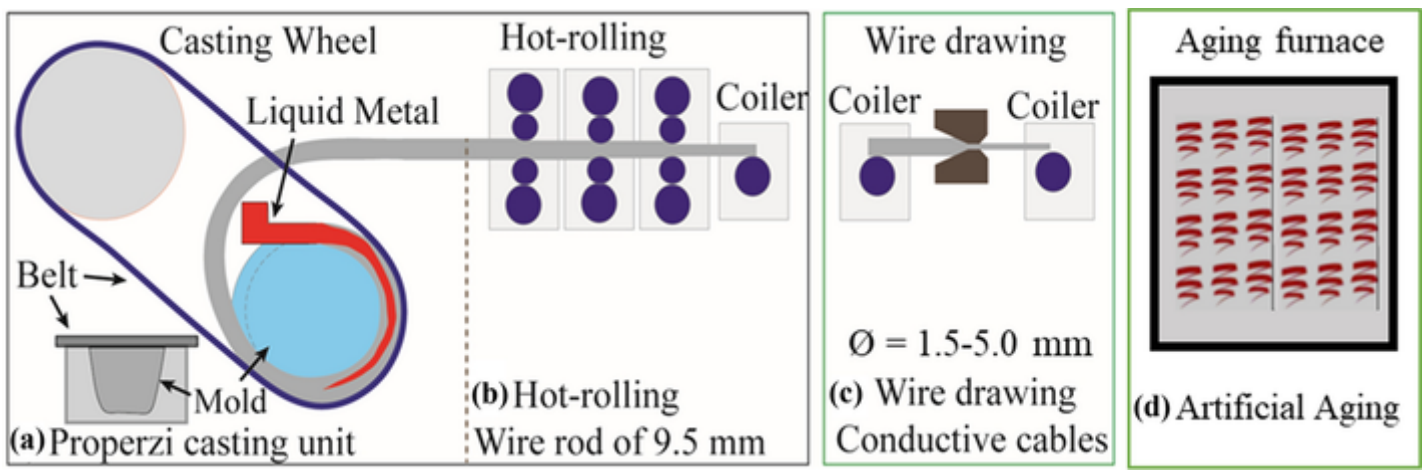

Effects of chemical composition on strength and EC

Principal alloying elements (Mg and Si)

Magnesium and silicon are known as the major alloying elements in 6xxx series alloys, leading to the precipitation of strengthening β''/β' phases during aging treatment. Therefore, it is initially valuable to address the effect of magnesium and silicon (or various Mg/Si ratios) on the strength and EC in these conductor alloys [24]. The precipitation sequence of the as-quenched 6xxx aluminum alloys is as follows: independent clusters of Mg and Si atoms → coclusters of Mg and Si atoms GP zones → β″ needle-like precipitates → β′ rod-shaped precipitates (and B′ lath-shaped precipitates) → equilibrium β-Mg_2Si [42, 43, 44]. The β″ precipitates are known as the main hardening phases in the peak-aged condition (T6). The MgSi phases are different with respect to their crystal structures and Mg/Si ratios. The Mg/Si ratios of these phases (in at.%) are as follows: β″ (Mg/Si ~ 1), β′ (Mg/Si ~ 1.7) and β (Mg/Si = 2) [44]. As mentioned above, the as-quenched materials are commonly drawn prior to aging treatment. Accordingly, the cold drawing after solution treatment could disturb the precipitation sequence due to the introduction of a large number of dislocations. Therefore, β″ formation could be suppressed, and the β′ phase was heterogeneously promoted along the dislocations [45, 46, 47]. Lath-like precipitates were also observed as the predominant microstructure feature, of which the crystal structure was similar to that of the β′ phase [45]. The precipitation sequences in the as-deformed condition became clusters/GP zones → β′ → equilibrium β-Mg_2Si [46, 47].

Xu et al. [24] reported the effect of different Mg/Si ratios on the strength and EC in as-drawn AA6101 conductor alloys, and the results are shown in Fig. 3 . The chemical compositions along with the Mg/Si ratio in the experimental alloys studied are listed in Table 1 . According to Xu et al. [24], an alloy with a Mg/Si ratio of 1.73 in wt% (2 in at.%) was considered a balanced alloy, although the Mg/Si ratio of the strengthening precipitates (β″) was approximately one (in at.%) [42, 44, 48, 49, 50, 51]. It is worth pointing out that the maximum solubilities of Mg and Si are 14.9 wt% at 449 °C and 1.65 wt% at 577 °C, respectively, and they are 1.7 wt% for Mg and trivial for Si at room temperature [52].

Figure 3

(a) Strength and (b) EC as a function of aging time at 180 °C. (c) strength versus EC for all aging times for 6101 alloy samples. Alloys #1 and #2 are the Si-excessive alloys, and alloys #3, #4, and #5 are the Mg-excessive alloys

Reprinted with permission from [24].

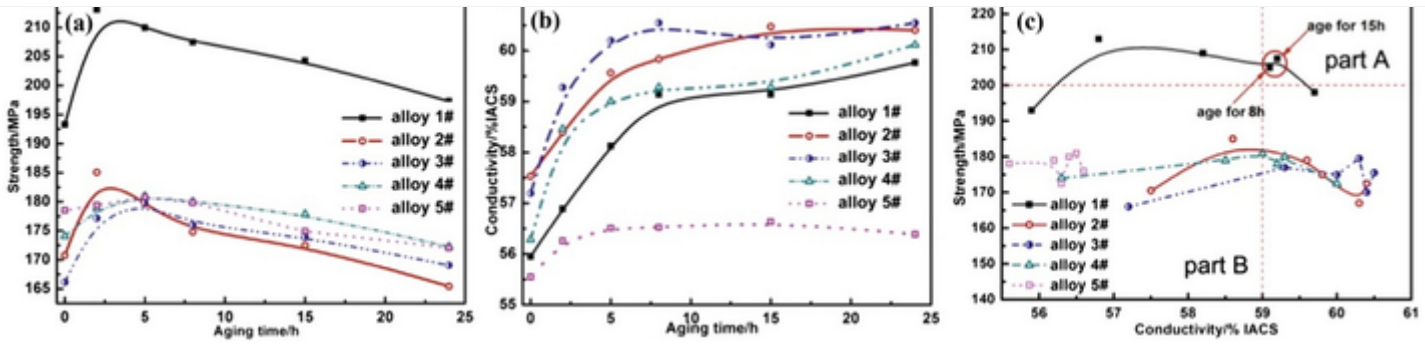

TABLE 1

Chemical composition (wt%) of the studied alloys

Reprinted with permission from [24].

Alloys	Si	Mg	Fe	Mg/Si	Types
1	0.49	0.58	0.18	1.18	Si excessive
2	0.39	0.59	0.19	1.51	Si excessive
Balanced	0.35	0.60	0.17	1.73	–
3	0.35	0.76	0.18	2.17	Mg excessive
4	0.35	0.86	0.18	2.46	Mg excessive
5	0.35	0.96	0.17	2.74	Mg excessive

Based on the results in Fig. 3, the higher the excessive Si level is, the faster the precipitation kinetics. Moreover, the peak strength was improved in Si-excessive alloys by 25%, which mainly resulted from a large number of strengthening precipitates, confirmed using DSC results and TEM analysis. However, excessive Mg exhibited no strengthening effect on the Al–Mg–Si conductor alloys [24, 25]. Moreover, Gupta et al. [53] also reported that the yield strength increased with increasing Si content. During the aging treatment, it was reported that the quenched vacancies were primarily trapped by Si atoms due to the higher diffusion rate, through which Si-rich clusters are formed. Subsequently, by slow diffusion of Mg atoms toward Si-rich clusters, Mg–Si clusters are formed [44, 54, 55]. This implies the key role of Si in the early stage of aging. Furthermore, Si_2 columns or Si grids as a skeleton of precipitates were observed in the core of precipitates from GP zones to β″ precipitates [49, 56, 57]. Moreover, it was detected that the Mg/Si ratio of strengthening phases decreased with increasing Si, indicating that the precipitation was closely connected with Si atoms rather than Mg atoms. As a consequence, precipitate strengthening was strongly governed by Si solutes in Al–Mg–Si conductors [58]. Although cold drawing might disrupt the precipitation sequence [45, 46, 47], excessive Si still exhibited a higher strength in as-drawn Al–Mg–Si conductor alloys [24, 26].

However, the Si-excessive alloy showed a relatively lower EC (Fig. 3b), which stems from Si solutes due to the larger difference in atomic radius of Al and Si [14, 24]. Although silicon has limited solubility in Al–Mg–Si alloys, DSC analysis confirmed that excessive Si remained in the aluminum matrix until the fully overaged state [59]. Therefore, optimized strength and EC were attained in the overaged condition after 8 h (Fig. 3c) in Si-excessive samples (alloy #1). Despite the longer time required for overaging, the Si-excessive sample presented a superior strength compared to the peak-aged strength of other samples (Fig. 3c). Excessive Mg alloys showed negligible superiority in strength. Alloy #5 (highly excessive Mg) exhibited the lowest EC due to the scattering electrons and had an insignificant impact on the strength [24]. Based on Fig. 3b, as the aging time increased, EC initially showed rapid growth and then moderately increased for all samples. An increase in EC could be attributed to the fact that the detrimental impact of precipitates on EC is inferior to that of solutes [24, 60].

In our recent work [26], the optimization of strength and EC was studied at different Mg/Si ratios for drawn wire samples (50% reduction). The sample with Mg/Si ~ 1 exhibited the highest strength among all samples with the minimum required EC (52.5% IACS). However, the sample with Mg/Si ~ 1.5 showed a better trade-off between strength and EC, provided EC is the main concern. The sample with Mg/Si ~ 0.86 (excessive Si) showed the highest peak strength. However, longer aging times were required to fulfill the minimum EC, giving rise to deterioration of precipitation strengthening and lower strength. Accordingly, the sample with Mg/Si~ 0.86 showed a limited window of hardness and EC [26, 27].

Jiang et al. [25] investigated the effect of the Mg/Si ratio on hardness and EC for ultrafine and coarse grain structures in Al–Mg–Si–Sc alloys aged at 200 °C. Figure 4 shows EC versus hardness for these conductors in terms of their best trade-off between hardness and EC. As observed in Fig. 4 for the coarse-grained structure, excess Si led to a higher hardness compared to excess Mg with a slight reduction in EC, which resulted from the promoted precipitation hardening. A high number density of precipitates with a spacing of several tens of nanometers might impair EC insignificantly. It is worthwhile to point out that the grain boundary precipitates barely formed in the coarse-grained Al–Mg–Si alloys. However, in the alloys with ultrafine grains, EC was more connected with the Mg/Si ratio, suggesting that excess Si led to a higher EC relative to excess Mg. Silicon promoted grain boundary precipitation, causing the depletion of dissolved Si and precipitates inside grains [25]. Silicon atoms diffuse toward grain boundaries to segregate, resulting in a depletion of Si within grains [15]. This is because the Si diffusion coefficient is larger than that of Mg, and the energy of the grain boundaries is high. Therefore, age softening took place in Si-excessive alloys with fine grains. In general, in ultrafine-grained structures, Si-excessive alloys displayed a

lower hardness than Mg-excessive alloys, resulting from the deterioration in age-hardening due to grain boundary precipitates [25]. Similar results were also seen for ultrafine-grained samples by Han et al. [15]. It was reported that the optimization of hardness and EC was achieved when the Mg/Si ratio of the alloy was 1.48. From Fig. 4, it is apparent that a competing approach is still attained between hardness and EC even with the different Mg/Si ratios in the coarse/fine-grained structures.

Figure 4

Hardness as a function of EC for Al–Mg-Si-Sc alloys with different grain size and Mg/Si ratio, of which the best hardness/EC combination is selected for all sets of samples. The line is a guide for the eyes

Reprinted with permission from [25].

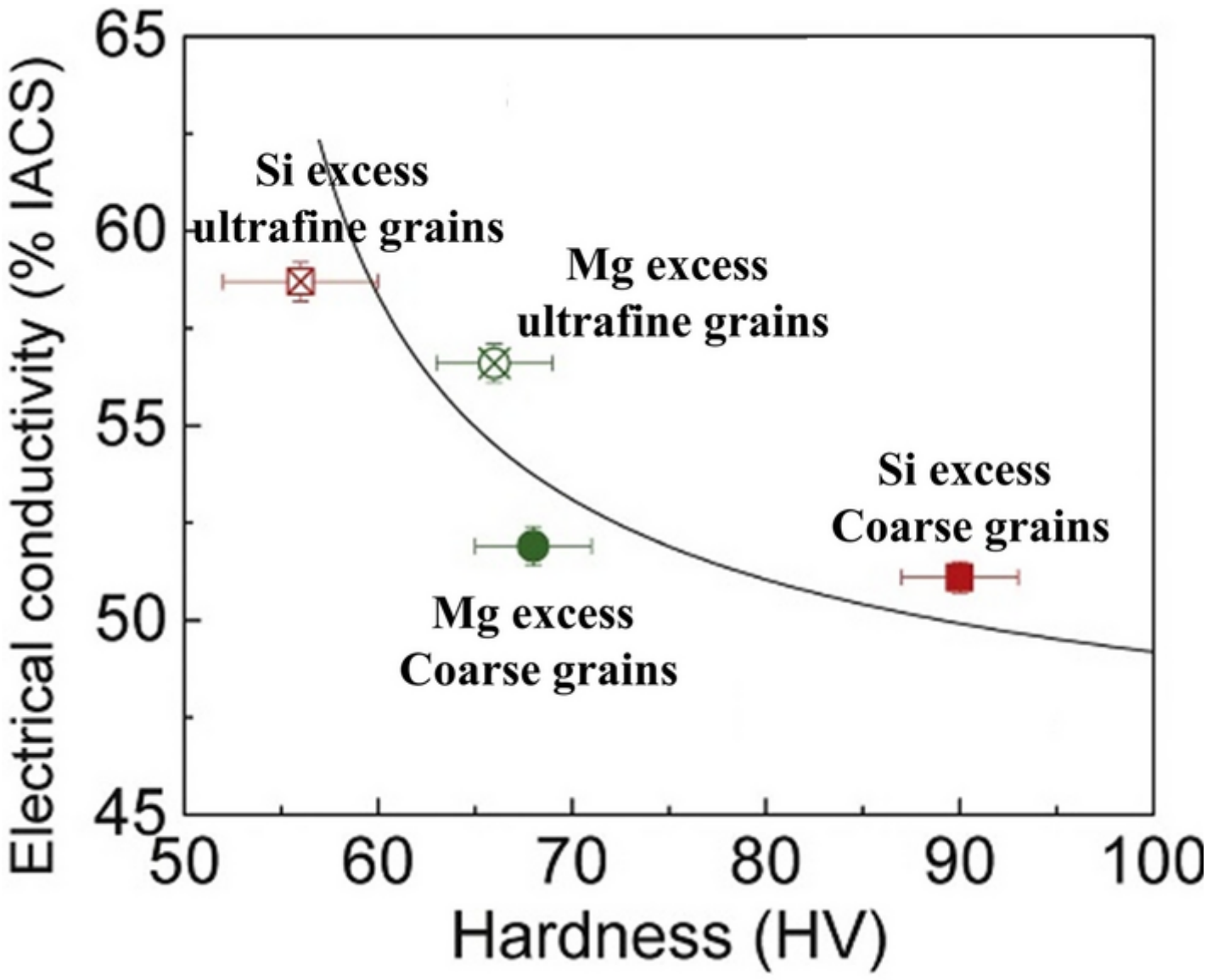

Smyrak et al. [61] also studied two alloys with different levels of Mg and Si while having the same Mg/Si ratio (~ 1): Al-0.72 Mg-0.71Si (HA) and Al-0.56 Mg-0.56Si (LA). The alloys were subjected to a solution treatment for 12 h at 550 °C, followed by natural aging for 24 h and then artificial aging at different temperatures (from 100 to 240 °C) and various time intervals (0–24 h); the associated results are displayed in Fig. 5. The data at high resistivity levels are attributed to aging temperatures less than 150 °C, and the data at low resistivity are ascribed to aging temperatures above 150 °C in both alloys. As shown in Fig. 5, an increase in Mg and Si elements (0.15 wt%) led to an increase in the strength by 25 MPa at the expense of EC (1 nmΩ). However, the HA alloy exhibited a higher strength at the high resistivity end relative to the LA alloy, presumably owing to a larger density number of precipitates in the HA alloy. It was reported that the optimal strength and EC (200 MPa–57.5% IACS) were acquired at 150 °C within 4–10 h for both alloys, which are favorable for the subsequent wire drawing to produce wires with high strength and high EC [61].

Figure 5

The relation between electrical resistivity and (a) yield strength (b) tensile strength for Al-0.72 Mg-0.71Si and Al-0.56 Mg-0.56Si alloys at different aging temperatures (100–240 °C) and various aging times (0–24 h)

Reprinted with permission from [61].

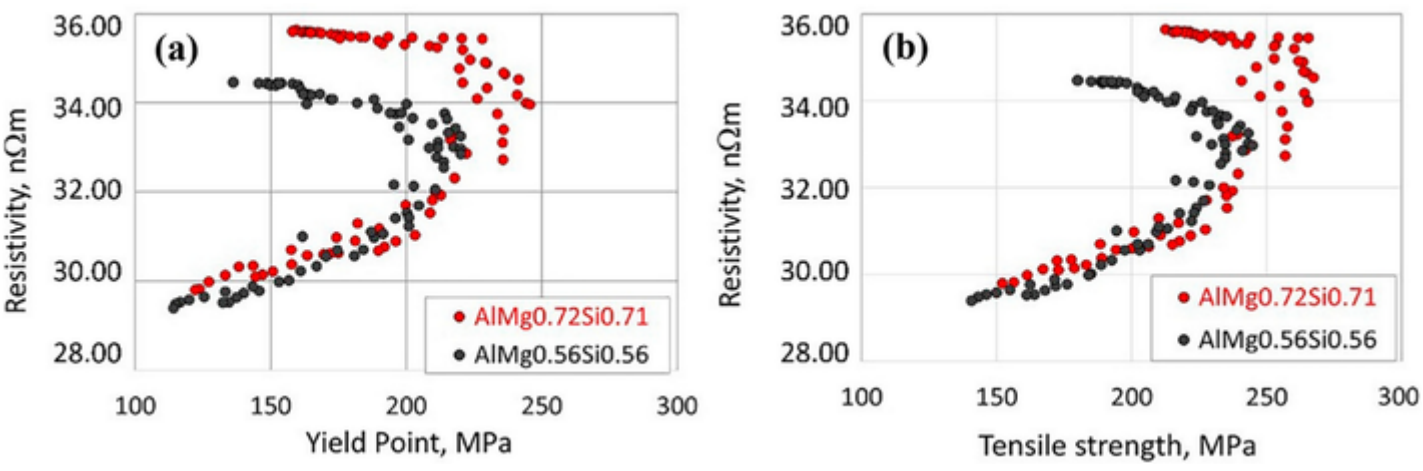

Additional alloying elements

Alloying elements and impurities that dissolve into the matrix as solute atoms have the strongest effects on electrical resistivity [14]. In addition, several alloying elements promote precipitation hardening [12, 28] in Al–Mg–Si alloys. Therefore, it is worth considering the effect of other alloying elements (aside from Mg and Si) on the strength and EC in Al–Mg–Si conductors. Among all alloying elements, transition elements exhibited the most detrimental impact on the EC (for example, Ti, Zr, V, Mn, Cr, and so on), as shown in Supplementary Fig. S2 [5, 6].

Zirconium is one of the most commonly used transient elements in aluminum alloys, affecting the mechanical and electrical properties. The results indicated that the mechanical properties were improved with Zr addition (Supplementary Table S2). The higher strength in the Zr-added alloy resulted from the presence of thermally stable Al_3Zr precipitates, which enhanced the strength via the Orowan mechanism. Moreover, these particles could retard recrystallization due to pinning the grain boundaries, which is known as the Zener pinning effect. Accordingly, the finer grain structure in the Zr-added alloy resulted in further strength improvement based on the Hall–Petch relation. It was also found that recrystallization could be prevented to some extent during solution treatment due to the presence of Zr precipitates [62, 63]. In contrast to strength, EC dropped in the presence of Zr due to the dissolved Zr solutes in the matrix and more grain boundaries (Supplementary Table S2) [62].

Lanthanum addition in AA6201 alloy exhibited a deterioration in the mechanical properties but an improvement in EC (Supplementary Table S3) [64]. Lanthanum led to the formation of $La(Al,Si)_2$, depleting Si in the remaining melt. Similarly, a reduction in the Si/Fe ratio in the melt favors the formation of the Chinese script α-AlFeSi phase [65]. Chinese script α-AlFeSi has a lower stress concentration relative to sharp needle-like β-AlFeSi phases, which is favorable for strength [66]. However, Si depletion gave rise to fewer precipitates. It was reported that La addition caused the strength to drop, which was attributed to the inferiority of fewer precipitates overcoming the superiority of Fe intermetallic modification on the strengthening. Improving EC with La addition was ascribed to a lower Si concentration in the matrix due to $Al\ (Si,\ La)_2$ formation [64].

Aside from lanthanum elements, the effect of cerium on the properties of Al–Mg–Si conductors was also investigated [67]. It was found that the Ce addition (0.3 wt.%) resulted in an EC improvement. This is because Ce in combination with Fe and Si forms AlFeSiCe compounds. Therefore, a reduction in Fe and Si levels in the matrix led to a higher EC [67]. However, Si consumption and depletion in the matrix reduced the precipitation response and strength.

The presence of Fe as an impurity is inevitable in aluminum alloys. Considering the low solubility of Fe in aluminum alloys, Fe generally exists as Fe-bearing intermetallic particles in the microstructure [66, 68]. It was reported that the addition of Fe increased EC, but decreased the strength (See Supplementary Fig. S3) [14]. Microstructural observations showed that with the addition of Fe, a continuous network of Fe-bearing intermetallics was formed in the as-cast structure. As Si atoms are usually integrated in solidified Fe-bearing intermetallics regardless of the Fe-bearing intermetallic type, the concentration of solute Si in the matrix is reduced, which favors EC improvement. However, a reduction in the Si level deteriorated the precipitation hardening, resulting in a lower strength [14, 69].

In contrast to transition elements, Sr addition was found to increase the strength in AA6201 alloy owing to intermetallic modification and a better response to aging [28, 66]. Regarding intermetallic modification, Sr addition stabilized Chinese script α-AlFeSi phases. Before going further, it is worthwhile to address the solidification reaction of AA6063, of which the chemical composition is in the similar range as that of the AA6101 alloy. The α-Al_8Fe_2Si intermetallic phase directly solidifies from liquid metal via a eutectic reaction, followed by a peritectic reaction in which L + α-Al_8Fe_2Si transforms into L + β-Al_5FeSi [68, 70]. Considering that the β-AlFeSi phase has a higher Si concentration than the α-AlFeSi phase, Si atoms from the liquid matrix must diffuse toward the α-AlFeSi phase to transform into β-AlFeSi in the peritectic reaction. With the addition of 30 ppm Sr, it was found that a large amount of Chinese script α-AlFeSi phases stabilized and did not transform into β-AlFeSi [66]. It was suggested that strontium adsorbed to the α phase interface, retarding Si diffusion and preventing the transformation of α-AlFeSi into β-AlFeSi in the peritectic reaction. The Chinese script α-AlFeSi phase possesses a desirable impact on the strength compared to sharp needle-like β-AlFeSi. This is related to the fact that α-AlFeSi intermetallics are compacted and have a lower stress concentration, thus improving the strength [66].

Regarding the better aging response, strontium could also improve the strength by ~ 15% by promoting the precipitation of as-drawn wires [28]. As a result of the prevention of β-AlFeSi transformation, more silicon remained in the matrix in the Sr-added AA6201 alloy since the α-AlFeSi phase contained less Si than β-AlFeSi. Subsequently, excessive silicon increased the precipitate density. The density number of precipitates in the Sr-added AA6201 alloy was approximately double compared to Sr-free AA6201 after 3 h of aging at 175 °C. However, the EC of the Sr-containing AA6201 alloy was lower than that of the Sr-free alloy, which was mainly attributed to more dissolved excess silicon [28]. It is worth mentioning that the Sr impact on the strength was maximized when the Fe level was relatively high (~ 0.3 wt%).

Flores et al. [12] investigated the effect of microalloying elements on the strength and EC of AA6201 using the optimized thermomechanical process, which is displayed in Fig. 6. The studied microalloying elements are Sr (0.003), In (0.01), Sn (0.013), Sb (0.05), Pb (0.08), and Bi (0.08) (all in wt.%). These amounts were chosen based on the maximum solid solubility of these elements in binary phase diagrams with aluminum. From the results in Fig. 6, Sn-alloy showed the highest strength (445 MPa) with low EC (48.2% IACS). However, the Bi-containing alloy exhibited a better trade-off between strength (426 MPa) and EC (52.7% IACS). Based on these results, the relation between strength and EC is similar to the trend shown in Fig. 1 for commercial aluminum alloys [12].

Figure 6

(a) A plot of strength and EC for AA6201 alloy with element additions for wires with 2.65 mm (width) square (b) enlarged view of (a) [12].

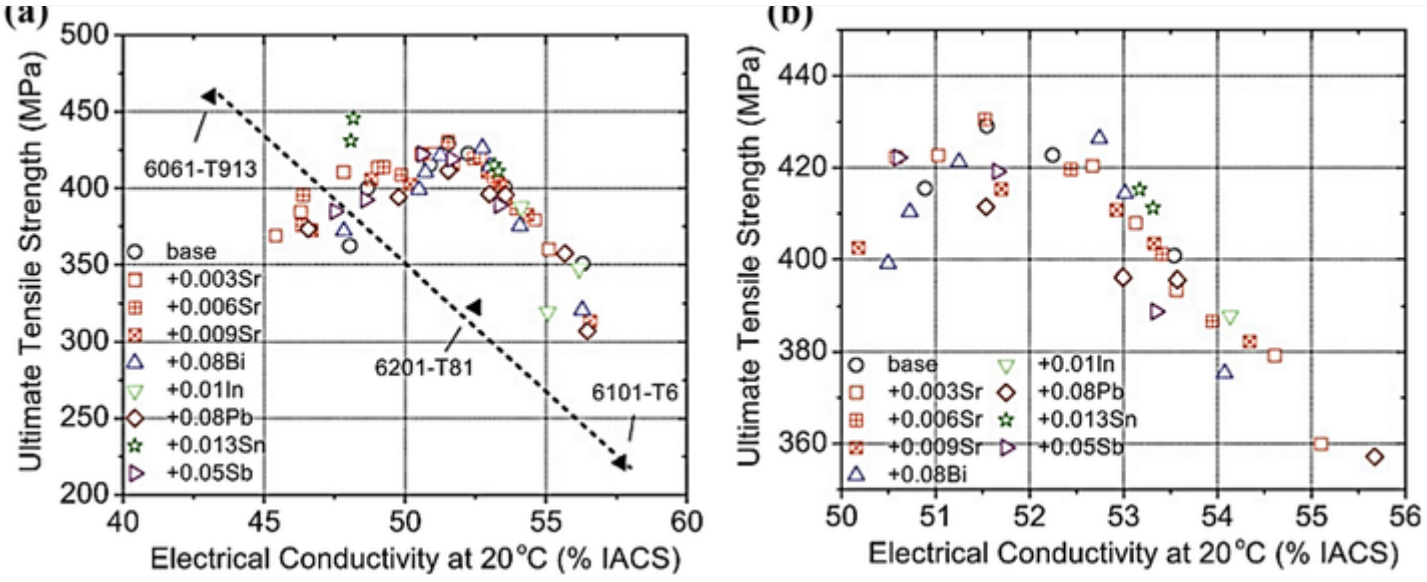

The addition of Cu and Ag to Al–Mg–Si alloys enhanced the response to age hardening [57, 71, 72]. To date, most studies have addressed the effect of Cu and Ag on the precipitation behavior and mechanical properties of Al–Mg–Si alloys. However, to the best of the authors' knowledge, no systematic studies have been found to determine the optimum level of the Cu and Ag in terms of the optimization of strength and EC in 6xxx conductor alloys.

Grain refiners and modifiers

The addition of grain refiners and modifiers (Al-B) is considered an important step during melt treatment in aluminum conductor fabrication, as mentioned in "Fabrication processes of 6xxx electrical conductors" section. The presence of dissolved transition metals (TMs) mostly leads to scattering electrons and deteriorating EC [5, 6, 29]. The EC-Grade commercial pure aluminum used for preparation of the 6101 conductor alloys contains 0.01Mn, 0.01V, 0.013Ti, 0.007Cr, and 0.006Zr (all in wt%) as impurities [5]. The boron addition in the form of Al-B master alloy removes the transition metals from the liquid metal by the formation of TM boride settling down in the tundish or furnace [5, 6], resulting in a remarkable EC improvement. Boron addition also enhances the resistance against failure of lightning arcs [5, 6, 29, 73]. The maximum efficiency of AlB_2 regarding a remarkable improvement in EC could be achieved in the first few minutes of AlB_2 addition (10% settlement of AlB_2) (See Supplementary Fig. S4a). It is also reported that that EC could be enhanced with boron excess up to 75%, above which EC is deteriorated (See Supplementary Fig. S4b).

In Al–Mg–Si conductor alloys, the combination of grain refiner and boron additions ought to be considered concurrently to achieve better electrical and mechanical properties. In Al-0.5 Mg-0.35Si conductor alloys, the addition of 0.12% boron (in the form of Al-3B master alloy) and 0.5% Al-5Ti-1B grain refiner resulted in a good combination of EC and strength in the as-cast condition [29]. The higher strength could be attributed to a fine grain structure based on the Hall–Petch relation, and the higher EC could stem from the extraction of transition elements via boron addition [29]. Accordingly, the addition of grain refiners and Al-B might lead to an enhancement of EC and strength in aluminum electrical conductors [29, 74]. Overall, the addition of a grain refiner (Al-Ti-B) improved the mechanical properties at the expense of EC. As a consequence, the amount of grain refiner (Al-Ti-B) should be as low as possible for refinement with the lowest detrimental effect on EC [29].

On the other hand, segregation of solute atoms and precipitates at grain boundaries could lead to an improvement in EC since more solutes could be extracted from the matrix [29]. Therefore, grain refinement is an important factor affecting precipitates and EC, although they have no direct influence on the precipitate crystal structure [72].

Effects of thermal and thermomechanical treatments on strength and EC

Thermomechanical treatments

As pointed out in "Fabrication processes of 6xxx electrical conductors" section, various thermal and thermomechanical treatments are applied to Al–Mg–Si conductor alloys during fabrication. Among those, thermomechanical treatments (i.e., aging and drawing processes) are the key tools to fulfil the requirements for strength and EC in overhead lines [12, 19, 30]. These processes could be optimized to maximize the strength via precipitation and strain hardening with a minimum loss in EC. It is of great technical interest to find a suitable approach to diminish the scattering of conducting electrons while the dislocation motions are significantly impeded. Hence, conventional and modified thermomechanical treatments will be addressed in the following sections.

Conventional thermomechanical treatments

Two important tempers are commonly used in conventional thermomechanical treatments for 6xxx series conductor alloys: T6 and T8 aging treatments. The T6 temper used for the AA6101 alloy consists of cold wire drawing, solution treatment and artificial aging, and the T81 temper employed for the AA6201 alloy is comprised of solution treatment, cold drawing, and artificial aging (Fig. 2) [12, 32]. A higher strength could be achieved via the T8 temper relative to the T6 temper, which is mainly derived from dislocation forests formed during wire drawing. The strain hardening associated with the drawing process could be entirely recovered through the applied solution treatment in the T6 temper [30]. The dislocations in the T8 temper led to a faster diffusion rate of solutes and coarsening of the precipitates during aging. Therefore, the coarse size and heterogeneous distribution of precipitates exhibited a lower degree of precipitation strengthening in the T8 temper [75, 76], which was counterbalanced with strain hardening from drawing. From the

viewpoint of EC, the T8 temper led to a higher increase in EC compared to T6 aging by depleting more solutes from the matrix into precipitates by dislocation-assisted diffusion [30]. Overall, the higher cold deformation in the wire drawing results in a higher peak strength at a shorter time since dislocations could promote precipitation kinetics [30, 77]. Accordingly, the required EC could also be achieved at a shorter aging time [7]. It can be inferred that the T8 temper ought to be used for the AA6201 alloy since it requires extracting more Mg and Si solutes from the matrix to enhance EC to the minimum required values.

The aging temperature (in T6 and T8) and the degree of cold deformation (in T8) in the drawing process are significant factors affecting the electrical and mechanical properties of conductors. With respect to the aging temperature, it was shown that the higher the aging temperature was, the higher the EC and the lower the strength at a given aging time [7, 60, 78]. At low aging temperatures, the minimum required EC might not be achieved, which could pertain to the remaining solute atoms in the matrix and the precipitates with a given interprecipitate spacing [7]. With respect to the deformation degree, it was seen that an increase in the degree of cold wire drawing could enhance strength due to strain hardening [79]. In addition, it was reported that high levels of Si and Mg could even lead to enhanced strain hardening [13]. The multiplication of dislocations during drawing only slightly deteriorates EC [79]. Moreover, the quantitative equation shows that a large number of dislocations have a negligible detrimental impact on EC [18, 26].

Despite extensive work carried out on the effect of various degrees of cold deformation (wire drawing) on EC and strength [30], microstructure investigations along with the underlying strengthening mechanisms are less reported in Al–Mg–Si conductors.

Natural aging (NA) is inevitable in conventional thermomechanical treatments during manufacturing Al–Mg–Si cables. After hot rolling in the Properzi process, the materials are exposed to mild quenching down to 50–65 °C, taking a few hours to reach room temperature [39]. Afterward, the materials are shipped to the customer plant to perform the wire drawing and aging process, experiencing several weeks of NA. Therefore, NA must be taken into account in terms of strength and EC. Rometsch et al. [79] investigated the effect of NA at the room temperature on the ultimate tensile strength (UTS) and EC in an Al-0.5 Mg-1.1Si alloy without any drawing processes, as shown in Fig. 7. The number of clusters and GP zones increased with prolonged NA, as seen in the images of the three-dimensional atom probe (3DAP) in NA at 1.1 h and 168 h, respectively. The formation of GP zones resulted in a higher strength and lower EC [39, 79]. NA gave an increase in the electrical resistivity due to the electron scattering of copious solute clusters and GP zones, while it slightly decreased the dissolved atoms in the matrix [79]. In addition, it was found that the NA samples showed a lower hardness in the postaging relative to the freshly quenched and aged sample (after 2 h aging) [79]. This is because the clusters and GP zones formed in NA were unstable, and they were dissolved into the matrix during artificial aging, ending with a low number density of precipitates in NA samples [80, 81].

Figure 7

Plot of EC and ultimate tensile strength of Al-0.5 Mg-1.1Si during various aging treatment without the drawing process [79].

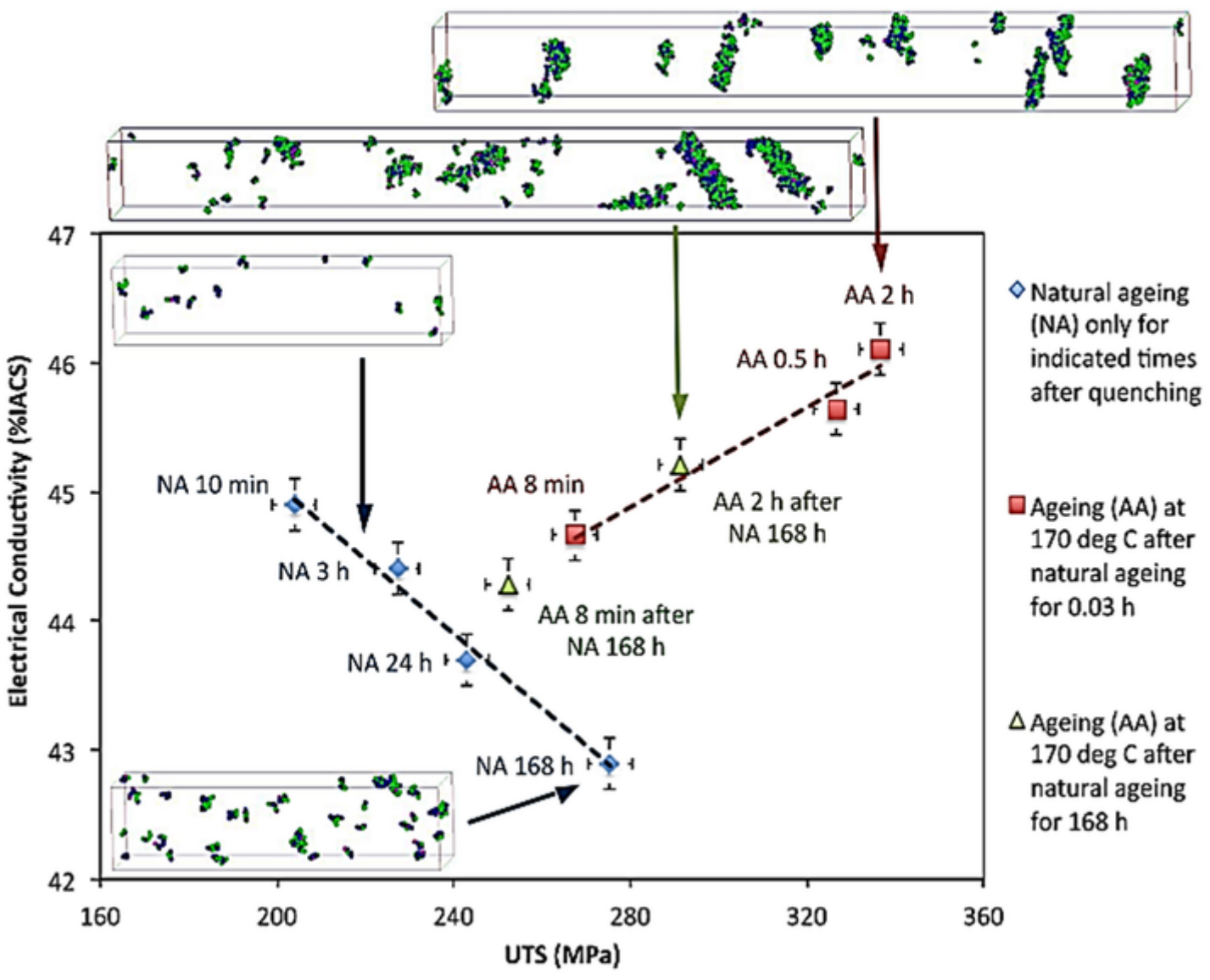

Practically, natural aging is followed by the wire drawing process [7, 39], meaning that the drawing process might affect clusters and GP zones formed during NA. Cervantes et al. [7] studied the effect of different NA times at room temperature followed by drawing and aging on strength and EC in AA6201 alloy containing 0.6 wt% Mg and 0.55 wt% Si. The NA samples showed a higher strength than the sample with no NA. Natural aging after 14 days followed by aging at 165 °C for 7 h exhibited the optimized strength and EC [7]. As

mentioned above, NA from mild quenching (down to 50–65 °C) followed by the subsequent storage at room temperature due to transportation should be also taken into account. In our recent work [37], the two-step natural aging was simulated and applied to the samples and compared with those without NA in terms of hardness (strength) and EC. The natural aging was comprised of solution treatment and quenching, 10 h or 20 h at 70 °C followed by keeping at ambient temperature for 2 weeks, drawing (50%) and aging (180 °C), designated as 10NA and 20NA samples, respectively. Figure 8 shows the plot of the strength and EC for the naturally aged samples (10NA and 20NA) and the samples without natural aging (No NA). The 10NA and 20NA samples exhibited a better compromise between strength and EC compared to No NA samples (Fig. 8). It should be noted that all samples exceeded the minimum required EC (52.5% IACS) after 5 h aging. The TEM micrographs of 20NA and No NA samples after 5 h aging are displayed in Fig. 9 to tailor the microstructural feature with the hardness values. The dominant microstructure in No NA samples is lath-like precipitates along with few needle-shaped precipitates extended in < 002 > Al direction (Fig. 9 a), shown with arrows in Fig. 9 a. In addition to these precipitates, the 20NA sample aged for 5 h revealed the precipitates with a smaller cross section shown with white arrows in Fig. 9 b. As shown in Fig. 9 d, the precipitate number density in the NA Samples is higher than those without NA owing to the presence of these fine precipitates. In the NA samples, the movement of the dense dislocations during wire drawing could shear and dissolve the GP zones into the matrix in the form of solute-enriched aggregates. Then, these aggregates evolved into these fine precipitates during postaging [37].

Figure 8

The plot of the strength and EC for samples with NA (10NA and 20NA), NA followed by preaging (20NA-PA), and without NA; all samples followed by cold wire drawing and aging at 180 °C

Reprinted with permission from [37].

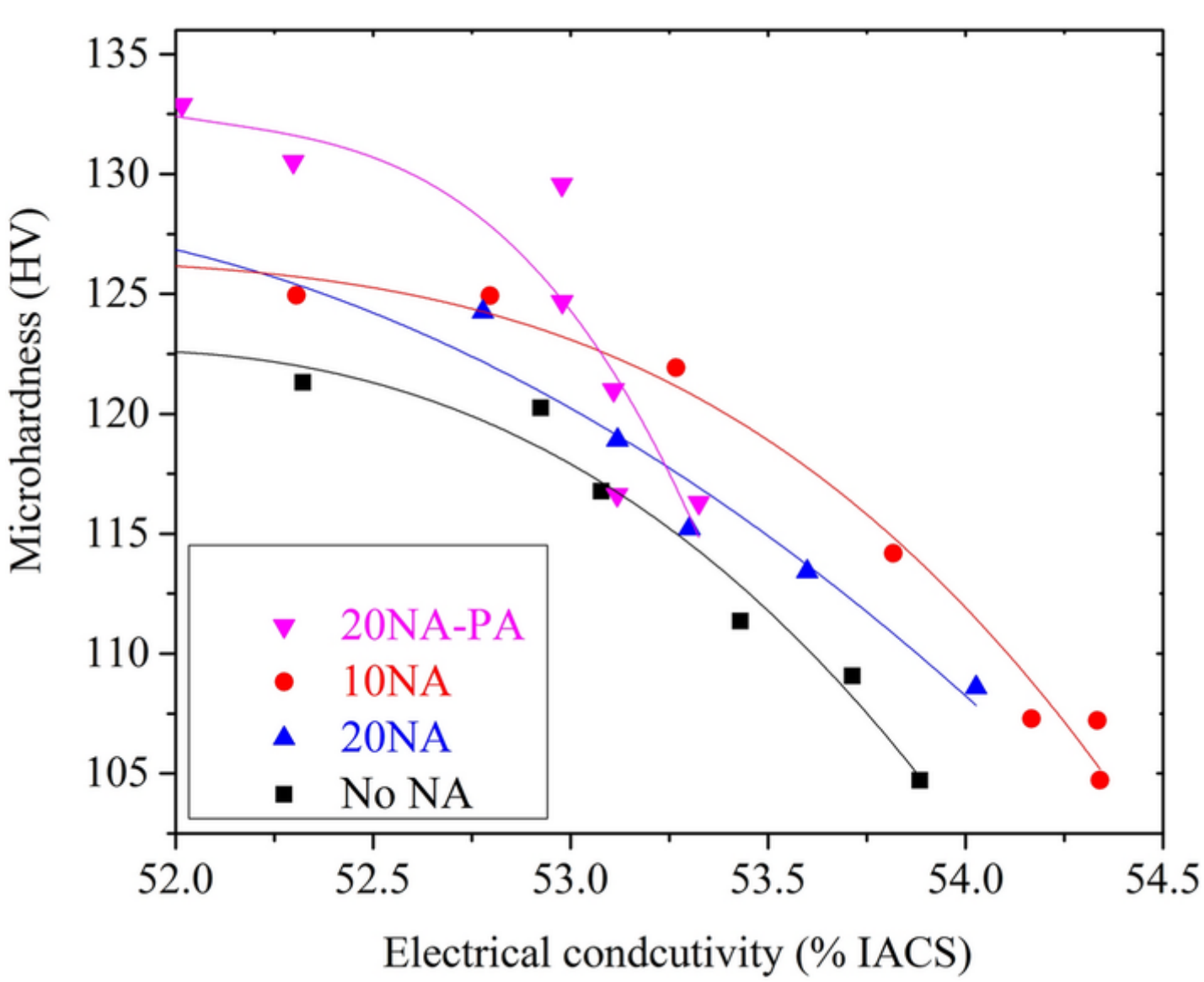

Figure 9

TEM images of (a) No NA sample aged for 5 h (b) 20NA sample aged for 5 h (c) 20NA-PA sample aged for 5 h, (d) the precipitate number densities, and (e) the average length and the cross section of precipitates. A and B correspond to the cross-sectional projections of lath-like and needle-shaped precipitates in < 002 > direction; C and D correspond to the longitudinal projections lath-like and needle-shaped precipitates, respectively. The specimen TEM samples were similar for the comparison

Reprinted with permission from [37].

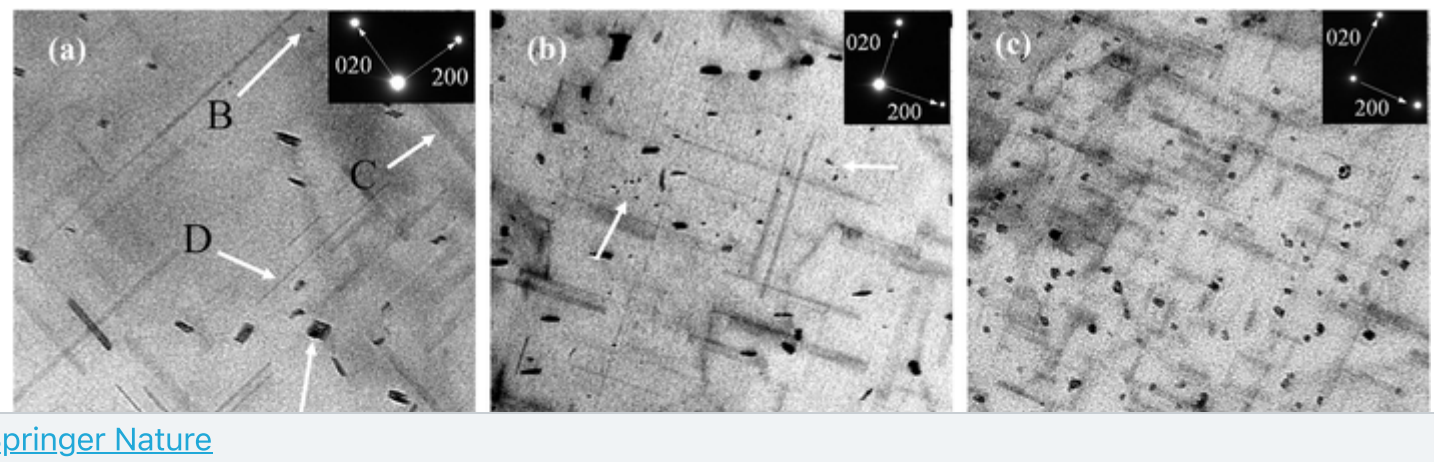

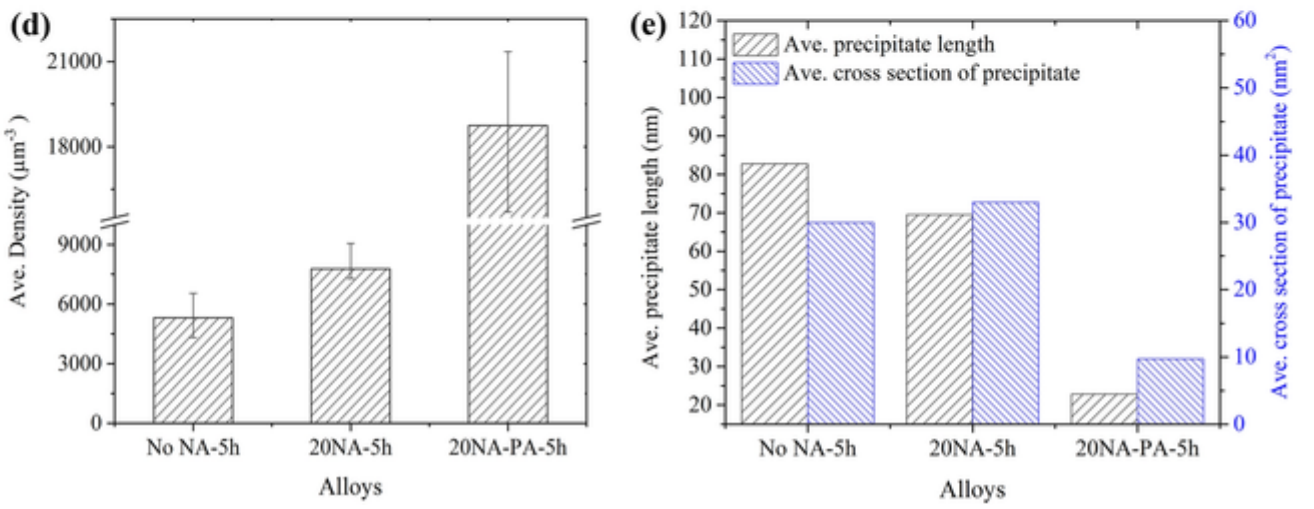

In Figs. 8 and 9, the 20NA-PA refer to the samples exposed to preaging (5 h at 180 °C) after the two-step NA, which will be discussed in the following section.

Modified thermomechanical treatments

High strength in Al–Mg–Si conductors is required for carrying loads caused by wind, ice and the weight of the conductor [32]. The proper design of thermomechanical treatments is among the techniques leading to the improvement of strength in conductors. A concurrent enhancement of the strength and EC could be obtained by changing the sequence of the thermomechanical process, known as modified thermomechanical treatments (M-TMT). In some M-TMTs, the sequence of the process consisted of solution treatment, preaging, cold drawing, and resuming artificial aging [19, 30, 31, 82, 83]. Preaging treatment can result in the formation of GP zones or precipitates.

Lin et al. [30] found that an M-TMT comprising a solution treatment, preaging for 2 h at 180 °C, cold rolling at a reduction of 70%, and reaging at 180 °C for 6 h exhibited a better combination of strength and EC (301 MPa and 58.9% IACS) for Al-0.62Mg-0.57Si alloy (in wt%) compared to the conventional thermomechanical treatment. It was observed that GP zones were formed during 2 h preaging, and they might be sheared off by dislocations in the cold rolling process. It was stated that the sheared GP zones could be subsequently dissolved in the matrix in the form of solute-enriched aggregates rather than homogeneously distributed solutes due to the low diffusion rate of solutes in cold rolling [30, 84, 85]. Then, the aggregates evolved into precipitates during reaging. Accordingly, more solute atoms were transformed into copious precipitates, leading to higher strength and EC [30]. Moreover, Bunte et al. [31] presented another M-TMT for AA6101 alloy, composed of partial aging at 200 °C for 1 h, wire drawing (65–90% cross section reduction), and reaging. This enhanced the strength (346 MPa), EC (53.5% IACS), and torsion properties, of which the underlying microstructure was not addressed [31].

Liu et al. [19] also suggested M-TMT for an Al-1Mg-0.5Si-0.8Cu alloy (in wt.%) to outperform conventional thermomechanical treatment (C-TMT). M-TMT consisted of solution treatment, preaging at 180 °C for 5 h, cold working (80% reduction) and resuming artificial aging (at 180–240 °C). The C-TMT was comprised of cold working (80% reduction), solution treatment and artificial aging (at 180–240 °C). Figure 10 displays the mechanical and electrical properties of Al–Mg–Si–Cu alloys treated by two different thermomechanical treatments. The strength and EC of the samples treated by M-TMT were higher than those of C-MTM. The higher strength of the samples in M-TMT could pertain to the high density of dislocations and precipitates. Notably, pre-existing precipitates formed during preaging were so stable during cold working, although their morphologies were slightly changed [19]. Notably, precipitate fragmentation was observed during plastic deformation owing to dislocation sliding [16, 86, 87]. In this M-TMT [19], the strength and EC reached 426 MPa and 53.5% IACS at 180 °C for 1 h, respectively. With further reaging (35 h), the strength and EC became 316 MPa and 57.4% IACS, respectively. An increase in EC with reaging time might mainly pertain to more precipitation of alloying elements from the matrix, through which the lattice distortion is mitigated. Conversely, prolonging the reaging caused the coarsening of precipitates, ending with a decrease in strength [19].

Figure 10

(a) Hardness vs. electrical conductivity in Al–Mg–Si–Cu alloys treated by C-TMT and M-TMT; (b) mechanical properties of the C-TMT and M-TMT samples reaged at 180 °C

Reprinted with permission from [19].

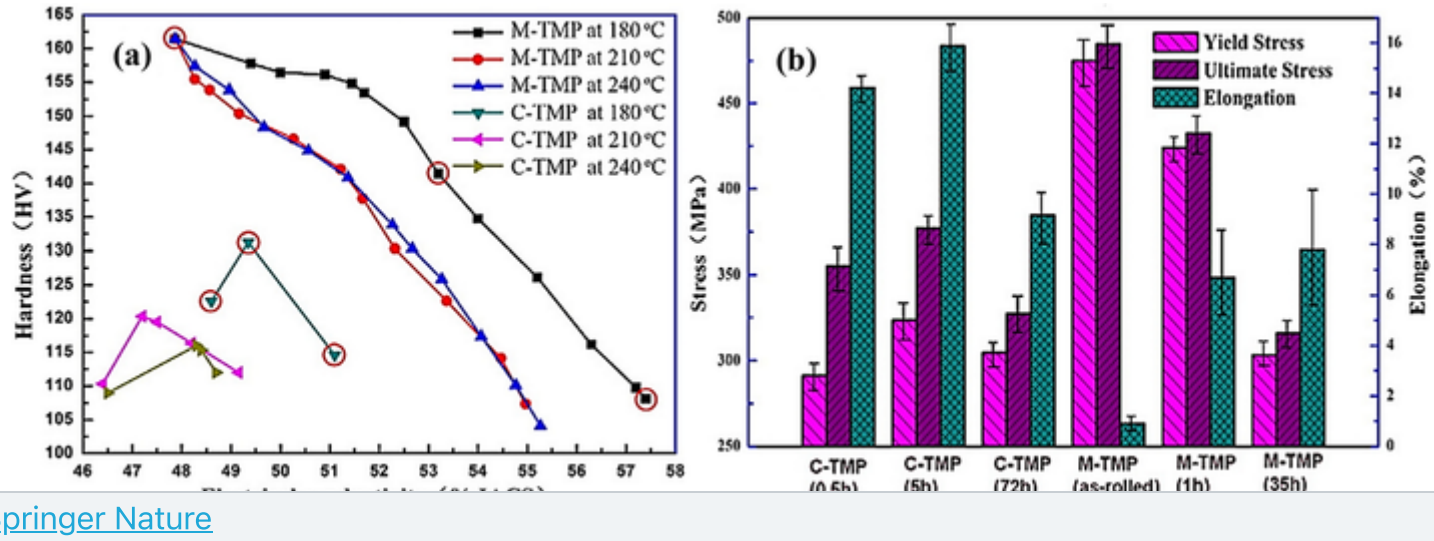

In M-TMT, it is often believed that the presence of precipitates could enhance strain hardening [30, 31]. In contrast, Cheng et al. [88] proved that the samples subjected to underaging and peak aging showed less strain hardening relative to the as-quenched samples in cold deformation.

In our recent work [37], preaging (5 h at 180 °C) was applied to the samples after two-step natural aging followed by the wire drawing and postaging, designated as 20NA-PA. As shown in Fig. 8, the 20NA-PA samples showed a better trade-off between hardness and EC compared to the NA samples and those without NA. The higher hardness above the minimum required EC (52.5% IACS) in the 20NA-PA sample was ascribed to their considerably higher number density of the precipitates relative to the other samples (Fig. 9). From Fig. 9, it appears that the pre-existing precipitates were fragmented during wire drawing via the moving dislocations, ended up with very short precipitates. Although the preaging maximized the precipitate hardening in the 20NA-PA sample, it deteriorated the strain hardening during wire drawing compared to the NA samples and those without NA. However, the increased precipitation hardening is superior to the reduced strain hardening in the 20NA-PA samples [37]. The microstructure evolution in the M-TMT 6101 alloys was also discussed in [89].

On the one hand, some studies [12, 32] have dealt with applying cold drawings after aging treatment, namely, first solution treatment, artificial aging at different times, and then cold wire drawing. Flores et al. [12] reported that an optimized route (solution treatment, aging at 200 °C, and wire drawing) for AA6201 alloy shows a better combination of strength and EC relative to T6 and T8 tempers. Furthermore, Hou et al. [32] also presented an M-TMT to obtain a better strength (352.3 MPa) and EC (56% IACS), which consisted of hot rolling at 390–420 °C followed by quenching, artificial aging at 175 °C for 4 h, and wire drawing. It is worth pointing out that the contributions of dislocation hardening and grain boundary strengthening were maximized in this process by omitting the conventional solution treatment. The higher strength of the AA6201 alloy processed by M-TMT was ascribed to the contribution of precipitation hardening, strain hardening, and grain boundary strengthening [32].

Martinova [83] also worked on an M-TMT, including 90–120 °C preaging for up to 1 h, cold drawing (75–95% reduction), and reaging at 170–200 °C. It was found that M-TMT exhibited a better compromise between strength and EC than conventional TMT.

In industrial practice, applying a solution treatment could cause extra cost and a complicated process [82]. Therefore, it is recommended to frequently regulate the temperature of the cast bar at the step before hot rolling to hold the temperature of the alloys above the solvus temperature during hot rolling [38]. Lentz et al. [82] suggested an acceleration of the cooling rate of solidification (> 100 K/s) for AA6101 alloy to retain Mg and Si in the matrix in twin-roll casting (TRC). The modified TRC was comprised of a high cooling rate from casting, 8 h aging at 185 °C, 80% cold rolling, and 8 h reaging at 185 °C (if necessary). This led to a strength of ~ 258 MPa with an EC of ~ 55.5% IACS in the as-rolled state and a strength of 211 MPa with an EC of ~ 57.5% IACS after reaging [82].

Other heat treatments

Aside from the aging treatment during the thermomechanical process, other heat treatments in the fabrication of conductor wires should be taken into account.

Yuna et al. [90] investigated the impact of homogenization temperature on the strength and EC in Al–Mg–Si–Ce conductor alloys. It was reported that it barely affected the strength of the alloy. However, rising the homogenization temperature from 535 to 560 °C led to an increase in EC from 56.5 to 57.3% IACS. With a further temperature increase up to 580 °C, EC slightly decreased to 56.8% IACS. In general, EC in the homogenized sample outperforms in the cast sample. The EC behavior as a function of homogenization temperature was attributed to the vacancy number. An increase in homogenization temperature from 535 to 560 °C augmented the vacancy number, leading to a smaller lattice distortion and higher EC. With a further increased in the temperature up to 580 °C, more vacancies could be formed. Then, the lattice parameter further decreased, and the lattice distortion generated again, deteriorating EC [90]. Karabay et al. [91] also found 560 °C as an appropriate homogenization temperature. In Al–Mg–Si conductor alloys containing 0.2 wt% Fe, both EC and strength were enhanced after homogenization at 630 °C for 8 h [14]. An improvement in strength could be associated with the formation of discontinuous rod-shaped α-Al_8Fe_2Si intermetallics with lower stress concentrations during high-temperature homogenization compared to plate-like intermetallics in the as-cast microstructure. In homogenization, some α-Al_8Fe_2Si intermetallics dissolved into the matrix at elevated temperature (630 °C), and then the dissolved Fe and Si atoms might extract out of the matrix toward the remaining α-Al_8Fe_2Si phase to decrease the volume and surface area of the phase, resulting in a discontinuous rod-shaped α-Al_8Fe_2Si phase [14].

The extrusion temperature could also influence the strength and EC of conductor alloys. Liao et al. [92] studied the electrical and mechanical properties of an as-extruded Al-0.35Si-0.2 Mg-0.3Ce alloy at different extrusion temperatures (460, 510 and 560 °C). The alloy extruded at 460 °C exhibited lower strength and higher EC relative to other extrusion temperatures. This extrusion temperature led to the dynamic precipitation of equilibrium noncoherent Mg_2Si particles. However, very weak dynamic precipitation could take place at 510 and 560 °C. Therefore, a lower strength at 460 °C was associated with a lower contribution of solute strengthening, and a higher EC pertained to the extraction of more solutes from the matrix [92]. In the solution heat treatment, the materials are kept at a temperature range between the solvus and the solidus line to dissolve solute atoms into the matrix [93]. In general, the extrusion temperature was recommended to be above 490 °C to achieve a favorable aging response [91]. Iraizoz et al. [9] reported 510 °C as the minimum solution treatment temperature for AA6201 (0.66% Mg, 0.53% Si and 0.20% Fe, in wt%) to maximize the age-hardening response. Indeed, the extrusion temperature is connected with the chemical composition of the samples since the alloy composition determines the solvus temperature.

Another heat treatment reported in the literature is intermediate annealing during cold wire drawing prior to aging. Wu et al. [94] investigated the effect of intermediate annealing during cold wire drawing on the mechanical properties and conductivity of an Al-0.2 Mg-

intermediate annealing was conducted at 150, 200, 250, 300 °C for an hour. Afterward, the rod was drawn to 3 mm at room temperature, followed by aging treatment. The highest strength (218 MPa) was achieved when the alloy was exposed to annealing at 150 °C for an hour. The strengthening effect of β" precipitates was superior to the softening impact at 150 °C. By increasing the annealing temperature to 300 °C, the strength dropped to some extent due to the softening effect originating from overaging, recovery, and recrystallization. In contrast, EC improved with increasing annealing temperature owing to solute extraction from the matrix [94]. Zhang et al. [95] also investigated the effect of annealing temperatures ranging from 200 to 500 °C for 3.5 h on the strength and EC in Al–Mg–Si alloy cables. It was shown that a higher annealing temperature increased the EC at the expense of strength due to recovery and recrystallization.

Osuch et al. [96] studied the effect of the direct aging procedure on the age-hardening response of AA6101. The procedure comprised solution treatment, followed by quenching in air down to the aging temperature and then immediate aging. Direct aging refers to precipitation during quenching in the air from the solutionization temperature to the aging temperature. Direct aging showed a higher EC at the expense of strength compared to conventional T6. This could stem from larger precipitates and a more precipitate-free zone formed in the direct aging procedure. A lower cooling rate during air quenching from the solutionization temperature to the aging temperature led to the diffusion of more vacancies toward grain boundaries. Therefore, vacancies were depleted in the vicinity of grain boundaries, resulting in the formation of a precipitate-free zone. EC enhanced with a slight drop in strength due to the formation of coarser precipitates. This heat treatment could be valuable if the EC might be taken as a priority over the strength [96].

Severe plastic deformation

Maximizing the area reduction in cold drawing might simultaneously enhance strength and EC. Therefore, new approaches have been developed to improve the strength and EC concurrently via severe plastic deformation (SPD) combined with artificial aging, lying strength and EC above the upper limit, as shown in Fig. 1 [16, 18, 35, 97]. The most well-known SPD processes are high-pressure torsion (HPT), equal-channel angular pressing (ECAP) and its modifications, accumulative roll bonding (ARB), and hydrostatic extrusion (HE) [98]. In the following section, various combinations of SPD processes and aging will be discussed in terms of electrical and mechanical properties.

Valiev et al. [16] found a desirable combination of strength and EC for AA6201 alloys using severe plastic deformation. In this study, HPT was initially performed at room temperature, followed by HPT processing at elevated temperatures (130, 180, and 230 °C). During HPT at elevated temperatures, a nanosized grain structure along with nanoscale precipitates formed. Therefore, the higher strength was attributed to grain boundary strengthening and precipitation hardening, and superior EC was ascribed to the absence of GP zones and fewer solutes. Based on the results in Supplementary Table S4, the best trade-off between strength (365–412 MPa) and EC (55.6–58.4% IACS) was achieved when the second HPT was performed at 130 and 180 °C. Similar results were also observed for AA6101 alloys by Sauvage et al. [18]. It is worthwhile to point out that precipitates were sheared by dislocations during SPD into spherical precipitates identified as β′-Mg_9Si_5 [16]. The strengthening effect of β′-Mg_9Si_5 precipitates could be ascribed to their small size (10–30 nm) and high number density. In addition, the lattice parameters of AA6201 at 130–230 °C were close to that of pure aluminum (4.0494°A), showing that most solute atoms were removed from the matrix into the β′-Mg_9Si_5 phase [16, 35, 97]. Indeed, the two-step SPD led to a decrease in GP zones and solute atoms in the matrix [16, 97]. The dynamic aging in the second SPD at 130–180 °C was a vital key to enhancing precipitation hardening and grain boundary strengthening. This is because ultrafine grains and precipitates were concurrently formed with few grain boundary precipitates [16]. The segregation of solutes and precipitates at grain boundaries could somehow assist EC enhancement [18]. In contrast, Jiang et al. [25] showed that grain boundary precipitates were the predominant microstructure feature after postaging of ultrafine-grained Al–Mg–Si conductor alloys, leading to higher EC at the expense of strength.

Sauvage et al. [18] showed the effect of HPT at room temperature followed by artificial aging on the hardness and EC in AA6101 alloys. Figure 11 a and b shows the variation in hardness and EC in the AA6101 alloy processed by 20 turns via HPT at room temperature followed by aging at different temperatures. Horizontal lines characterized conventional T4 (natural aging) and T6 (peak hardness) treatments of the same alloy. Based on Fig. 11 a and b a good combination of hardness and EC was achieved at 130 °C owing to grain boundary strengthening and precipitation hardening. Precipitates were observed both at grain boundaries and inside grains in these samples. The AA6101 alloy treated by HPT at room temperature and aging at 100 and 130 °C showed hardness levels 20% higher than those of the T6 alloy at the end of aging (Fig. 11 a) [18].

Figure 11

(a) Microhardness (b) EC for AA6101 processed by HPT at room temperature followed by artificial aging at various temperatures. Microhardness of the sample for T4 and T6 tempers are brought for comparison purpose. Reprinted with permission from [18]. (c) A comparison of strength and EC for (AL2–AL7) in EN 50,183 standard (green box) with those obtained by severe plastic deformation (red box) for AA6201 alloy

Reprinted with permission from [16].

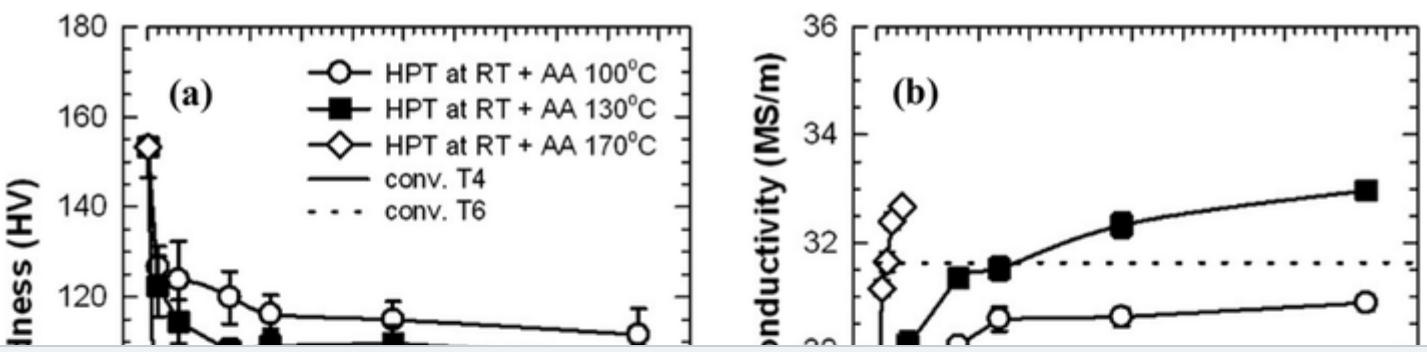

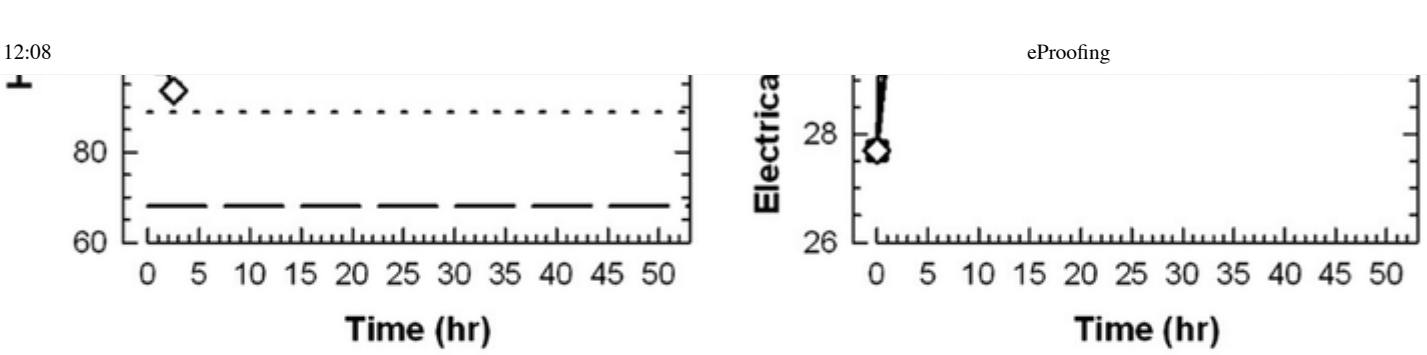

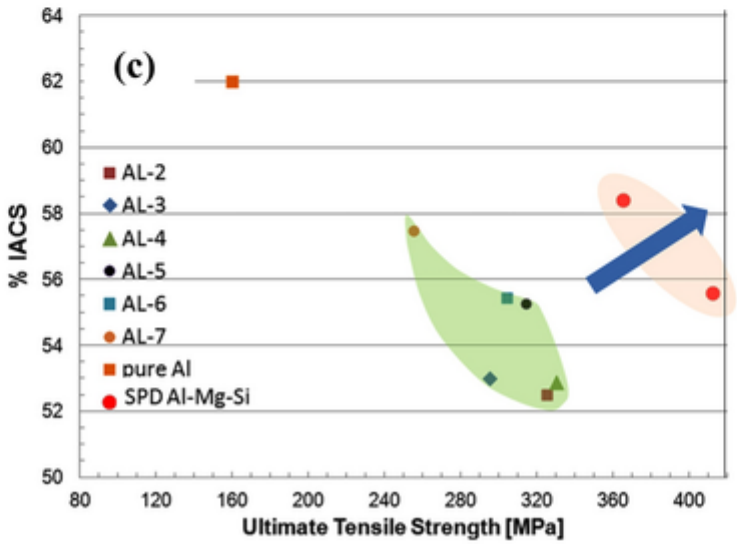

Murashkin et al. [34] also reported a better combination of strength and EC for AA6101 alloys using equal-channel angular pressing with parallel channel (ECAP-PC) processing above 100 °C followed by artificial aging. The main drawback of HPT and ECAP-PC (as SPD processes) is the small size of billets, limiting their application in the industry. Murashkin et al. [35] presented equal-channel angular pressing-Conform (ECAP-C) producing an electrical wire from long billets. High EC (57.1% IACS) and strength (over 304 MPa) of AA6101 alloy could be achieved using (ECAP-C) at 130 °C followed by aging at 170 °C for 12 h. In this process, EC and elongation were higher than those reached at T81 process while strength is similar. As mentioned for SPD via HPT, (ECAP-C) at 130 °C also led to dynamic aging. Postartificial aging improved EC via precipitation with a slight decrease in strength. The β' phase precipitated along grain boundaries via dynamic aging in ECAP-C at 130 °C. In addition, some β' precipitates formed inside grains in subsequent artificial aging [35].

Figure 11 c illustrates the relation between the strength and EC for Al–Mg–Si conductors. The green box in the figure is related to conventional Al–Mg–Si conductors (EN 50183 standard), while the red box belongs to AA6201 alloy with nanosized grains and nanoscale precipitates achieved by SPD [16]. The same trend was observed for AA6101 alloy [18]. Severe plastic deformation along with aging results in the strength and EC above the upper limit for commercial aluminum conductors.

Majchrowicz et al. [33] studied hydrostatic extrusion (HE) combined with artificial aging, which could be applicable for the fabrication of electrical wires via long billets. It improved the strength owing to grain boundaries and precipitate strengthening with a relatively high EC for the AA6101 alloy. In the process after solution treatment, the materials were subjected to the HE extrusion process, of which the diameter was reduced from 20 to 10 mm, designated H10. Afterward, these extruded materials were re-extruded down to diameters of 4 mm and 3 mm, designated H4 and H3, respectively. Finally, artificial aging was performed at 180 °C for 1–24 h. Figure 12 demonstrates the evolution of strength and EC as a function of aging time for HE-processed AA6101 and coarse-grained (CG) AA6101. Based on the results, hydrostatic extrusion led to a shorter aging time for peak hardness, meaning that precipitation kinetics were increased due to microstructural defects acting as nucleation sites for precipitates. Notably, adiabatic heating during extrusion caused the temperature to increase up to 150 °C, leading to the formation of GP zones during hydrostatic extrusion. The electrical conductivities of H3 and H4 of AA6101 were found to be much higher than those of CG AA6101. Grain boundary segregation and precipitates in extruded AA6101 gave rise to more matrix purification. HE4 of AA6101 aged at 180 °C for 7 h was identified as the best compromise between EC (58% IACS) and strength (332 MPa). Some spherical (β'-$Mg_{1.8}Si$ or β-Mg_2Si) precipitates were observed at grain boundaries, showing overaged conditions. Hydrostatic extrusion followed by artificial aging exhibited a better combination EC and strength in comparison to the values in the EN 50183 standard [33]. As mentioned above, postartificial aging of ultrafine-grained Al–Mg–Si alloys most improved EC at the expense of strength due to more grain boundary precipitation [33].

Figure 12

(a) Hardness (b) EC for AA6101 exposed to different hydrostatic extrusion (HE) reductions and aged at 180 °C up to 24 h

Reprinted with permission from [33].

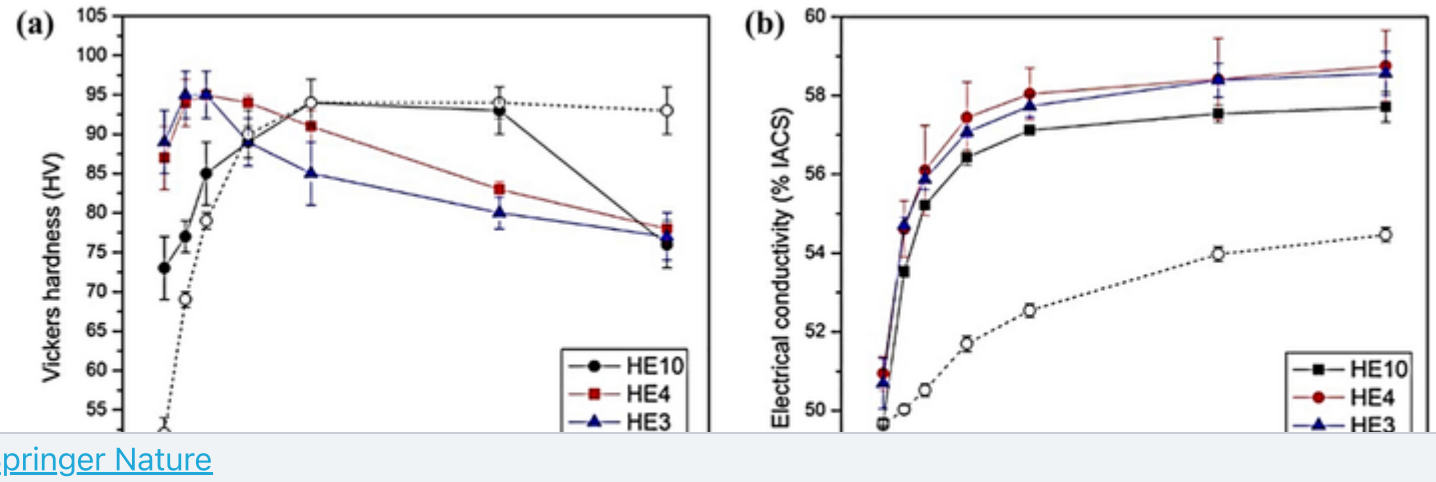

Medvedev et al. [99] applied ECAP to solutionized AA6101, followed by aging at 130 °C for up to 72 h. ECAP was applied for 2, 4, and 8 passes, corresponding to strains 2.3, 4.6, and 9.2, respectively. Figure 13 displays the EBSD images of the samples after 2, 4, and 8 passes without and with aging treatment. It could be deduced that an increase in the number of ECAP passes to 4 passes resulted in thickening shear bands (Fig. 13 b). With a further increase in the number of ECAP passes to 8 passes, the shear band became thin (Fig. 13 c). This was attributed to the dynamic recovery process at high deformation because a high dislocation density facilitates the transformation of dislocation arrays into high-angle grain boundaries. The microstructure just after the ECAP process was not uninformed and comprised intersecting shear bands with small grains of ~ 200 nm inside and an interband matrix containing large grains of ~ 10–20 µm. Figures 13 d to 13f show the microstructures of samples after aging at 130 °C after 72 h for 2, 4, and 8 passes. Samples after aging tended to form uniform equiaxed grains due to dynamic recrystallization (DRX). The lower degree of equiaxed grains after 2 passes of ECAP and aging (Fig. 13 d) might be attributed to the lower level of strain, which was not sufficient for dynamic recrystallization [99].

Figure 13

EBSD microstructure images of AA6101 Alloy after 2, 4, and 8 passes of ECAP-BP (a–c) without aging, (d–f) BP after aging at 130 °C for 72 h, in the sample cross section

Reprinted with permission from [99].

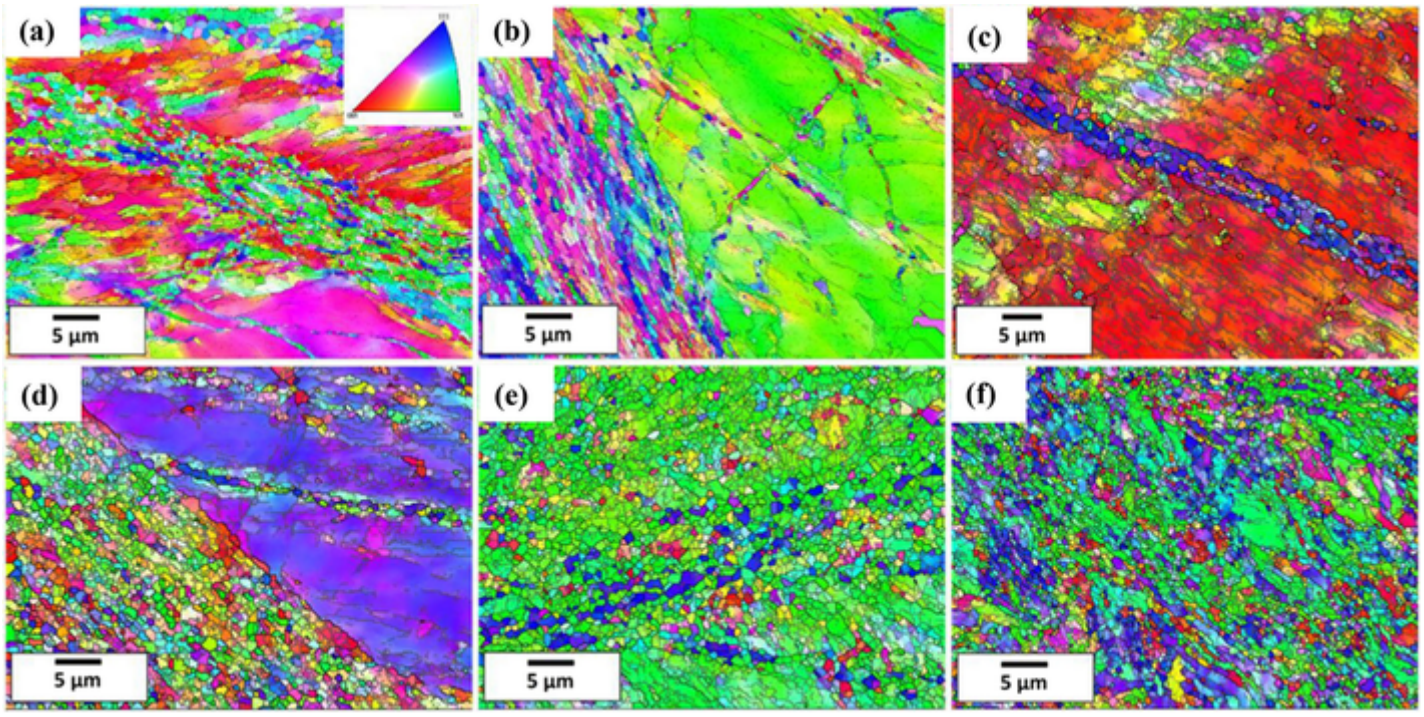

Recent development in modeling Al–Mg–Si conductor properties

Strength model in Al–Mg–Si alloys

As mentioned above, the main strengthening mechanisms in Al–Mg–Si alloys are precipitate strengthening, dislocation strengthening, grain boundary hardening, and solid solution strengthening. In general, the total strength equals the linear sum of strengthening mechanisms by assuming that they are independent, as expressed in Eq. 1 [15, 18, 25, 100, 101].

$$\sigma_{\text{total}} = \sigma^{\text{Al}} + \Delta\sigma^{\text{PREC}} + \Delta\sigma^{\text{DISLO}} + \Delta\sigma^{\text{GB}} + \Sigma\Delta\sigma_i^{\text{SOL}}, \quad (1)$$

where the σ_{total} is the total strength, σ^{Al} is the strength of the aluminum matrix, $\Delta\sigma^{\text{PREC}}$ is precipitate hardening, $\Delta\sigma^{\text{DISLO}}$ is strain hardening via dislocation forest, $\Delta\sigma^{\text{GB}}$ is grain boundary strengthening, and $\Sigma\Delta\sigma_i^{\text{SOL}}$ is the solute strengthening of elements dissolved in the aluminum matrix.

Precipitation of β″/β′ is the most prominent strengthening factor in heat-treatable Al–Mg–Si alloys owing to their age-hardening response. Depending on the precipitate types, the dislocation sliding is hindered by either shearing or bypassing of precipitates [100].

For shearable precipitates (β″), the increased strength could be expressed by the following equation (Eq. 2) [100].

$$\Delta\sigma_{\text{shear}}^{\text{PREC}} = \frac{M}{(b^2\sqrt{\beta G})}(N_y \cdot r_p)^{1/2} \cdot F^{3/2}, \quad (2)$$

$$F = 2\beta G b^2 \cdot \left(\frac{r}{rc}\right), \quad (3)$$

where β is a constant close to 0.28, M as Taylor factor is taken as 2 [102, 103] or 3 [18, 25] to convert shear stresses into normal stresses, G is the shear modulus (26.9 GPa) of FCC Al, and b is the burger vector (0.29 nm) of the dislocations in FCC Al(110) [18], Nv is the volume density of precipitates, r_p is the mean size of precipitates, rc is the transition radius from precipitate shearing to bypassing (5 nm), and F is the mean obstacle strength of precipitate [100].

For non-shearable precipitates (β′), the stress required to bypass the precipitates (Orowan mechanism) can be given in Eq. 4 [15, 18, 25].

$$\Delta\sigma_{\mathrm{Or}}^{\mathrm{PREC}} = \frac{2M\beta Gb}{L^{\mathrm{PREC}}}, \quad (4)$$

L^{PREC} is defined as the mean particle spacing, expressed in the following equation [18].

$$L^{\mathrm{PREC}} = \frac{1}{(Nv)^{1/3}}, \quad (5)$$

It is worth mentioning that the strength at the minimum required EC (52.5% IACS) for AA6201 alloy was usually achieved in the overaged condition [21]. Then, the Orowan equation was generally fitted with the precipitate strengthening model [15, 18, 25].

Strain hardening via dislocation forest is also considered as a significant strengthening factor in Al–Mg–Si conductors due to the cold deformation process. Equation 6 could be used to estimate the strain hardening as a function of dislocation density [15, 18, 25, 100].

$$\Delta\sigma^{\mathrm{DISL}} = \alpha.M.G.b.(L^{\mathrm{dislo}})^{1/2}, \quad (6)$$

where M, G, and were defined above; α is a constant close to 0.3, and L^{dislo} is the density number of dislocations measured using X-ray diffraction [18].

The strength provided by grain boundaries is expressed by the well-known Hall–Petch equation (Eq. 7) [15, 25].

$$\Delta\sigma^{\mathrm{GB}} = k_{\mathrm{HP}}d^{-1/2}, \quad (7)$$

where k_{HP} is a scaling constant (0.042 MPa/m$^{-1/2}$), and d is the mean grain size of the samples [25].

The increased hardness due to the solutes (particularly Mg and Si) could be estimated using Eq. 8 [15, 18, 25, 101].

$$\Delta\sigma^{\mathrm{SOL}} = \sum k_i C_i^{2/3}, \quad (8)$$

where $\Delta\sigma^{\mathrm{SOL}}$ is the increased hardness value for solute i, and k_i is a scaling factor for the solute i, for instance. 29 and 66.3 MPa (wt%)$^{-2/3}$ for k_{Mg} and k_{Si}, respectively. C_i is the concentration of the solute i (in wt%) [15, 18, 25, 101].

Electrical resistivity model

As discussed in "Introduction" section, the electrical resistivity is closely connected with the crystal defects. Accordingly, in Al–Mg–Si conductor alloys, the total electrical resistivity could be estimated by summing the resistivity contributions in a linear manner (Matthiessen's rule), as given in Eq. 9, which could be converted to the electrical conductivity (% IACS) using Eq. 10. Matthiessen's rule is the most common and used modeling to estimate the electrical resistivity from the different resistivity contributions. However, this model does not consider the interaction of each resistivity factors on each other, and resistivity factors are independently considered [104].

$$\rho_{\mathrm{total}} = \rho^{\mathrm{Al}} + \Delta\rho^{\mathrm{PREC}} + \Delta\rho^{\mathrm{DISLO}} + \Delta\rho^{\mathrm{GB}} + \Delta\rho^{\mathrm{SOL}}, \quad (9)$$

$$EC(\%\mathrm{IACS}) = \frac{172.4}{\rho^{\mathrm{total}}(\mu\Omega\mathrm{cm})}, \quad (10)$$

where the total resistivity (ρ_{total}) can be calculated by the summation of the resistivity from the aluminum matrix (ρ^{Al}), precipitates ($\Delta\rho^{\mathrm{PREC}}$), the dislocation forest formed via the cold wire drawing ($\Delta\rho^{\mathrm{DISLO}}$), grain boundaries ($\Delta\rho^{\mathrm{GB}}$), and the solutes ($\Delta\rho^{\mathrm{SOL}}$).

The electrical resistivity of precipitates is estimated using Eq. 11 [105]. The minimum EC generally is acquired in the overaged condition, and precipitates are less coherent with the matrix in the overaged condition. Besides, Eq. 11 does not consider the coherency of precipitates with the matrix, which might be a limitation for Eq. 11. Therefore, it is assumed that the mean particle spacing is the controlling factor on the precipitate resistivity.

$$\Delta\rho^{\mathrm{PREC}} = \frac{\Delta\rho^{\mathrm{prec}}}{(L^{\mathrm{prec}})^{1/2}}, \quad (11)$$

where $\Delta\rho^{\mathrm{prec}}$ is the resistivity constants (12 Ω(nm)$^{3/2}$) for the precipitates in the aluminum matrix [105].

Equation 12 could be used to estimate the electrical resistivity caused by dislocations [18].

$$\Delta\rho^{\mathrm{DISL}} = L^{\mathrm{dislo}}\Delta\rho^{\mathrm{dislo}}, \quad (12)$$

$\Delta\rho^{\mathrm{dislo}}$ is known as a resistivity constant of dislocation (2.7×10^{-25} Ωm^3) [18].

The grain boundary resistivity could be estimated by Eq. 13 [18].

$$\Delta\rho^{GB} = S^{GB}\Delta\rho^{gb}, \quad (13)$$

where $\Delta\rho^{gb}$ is the resistivity constants for grain boundaries (2.6×10^{-16} Ωm^2). S^{GB} is defined as $6/d$ (d is the average grain size). The grains are preferentially elongated in the microstructure in the wire drawing direction. However, in Eq. 13, it is supposed that grains are spherical to calculate the grain boundary resistivity ($\Delta\rho^{GB}$), which might be considered as a limitation for this equation [18].

The increased electrical resistivity due to the solutes could be estimated using Eq. 14 [18].

$$\Delta\rho^{SOL} = \sum C_i^{sol}\Delta\rho_i^{sol}, \quad (14)$$

where $\Delta\rho^{SOL}$ is the resistivity contribution due to solutes and $\Delta\rho_i^{sol}$ is the resistivity constants for the solute i. For Mg and Si solutes, $\Delta\rho^{Mg-sol}$ and $\Delta\rho^{Si-sol}$ are 0.445×10^{-6} Ωcm (at.%)$^{-1}$ and 0.496×10^{-6} Ωcm (at.%)$^{-1}$, respectively [18].

Case study of strength and electrical resistivity models

It would be valuable to estimate the effect of various strengthening factors on the strength and electrical resistivity of aluminum conductor alloys using the models and constitutive equations described above. This will provide a great aid to design a proper thermomechanical treatment with the appropriate addition of alloying elements. In this case study, some assumptions in the microstructure and alloying elements in an Al–Mg–Si alloy (AA6201) were considered to demonstrate the impact of strengthening factors. Here, it is supposed that the microstructure of an AA6201 alloy containing 0.6% Mg and 0.6% Si (all in wt%) is characterized by a mean particle spacing of 50 nm for β′ precipitates, a dislocation number density of 10^{15} m^{-2}, and a mean grain size of 400 nm in the case of ultrafine grains obtained by severe plastic deformation. It is worth mentioning that the strengthening mechanisms are considered independent of each other.

It is assumed that the mean particle spacing is 50 nm, and the Taylor factor is taken as 2. Given that a desirable EC was typically achieved in the overaged state [18, 33], the contribution of β′ precipitates to the strength and electrical resistivity could be calculated using Eqs. 4 and 11, which are determined to be 175 MPa and 1.69 nmΩ, respectively, as shown in Fig. 14. It is evident that the mean particle spacing of precipitates is a key factor influencing the strength and electrical resistivity of the Al–Mg–Si conductor alloy.

Figure 14

The contribution to the strength and electrical resistivity from precipitates (mean precipitate spacing = 50 nm), dislocations (density = 10^{15} m^{-2}), grain boundaries (grain size = 400 nm), and solutes (Mg = 0.3 wt% and Si = 0.3 wt%).

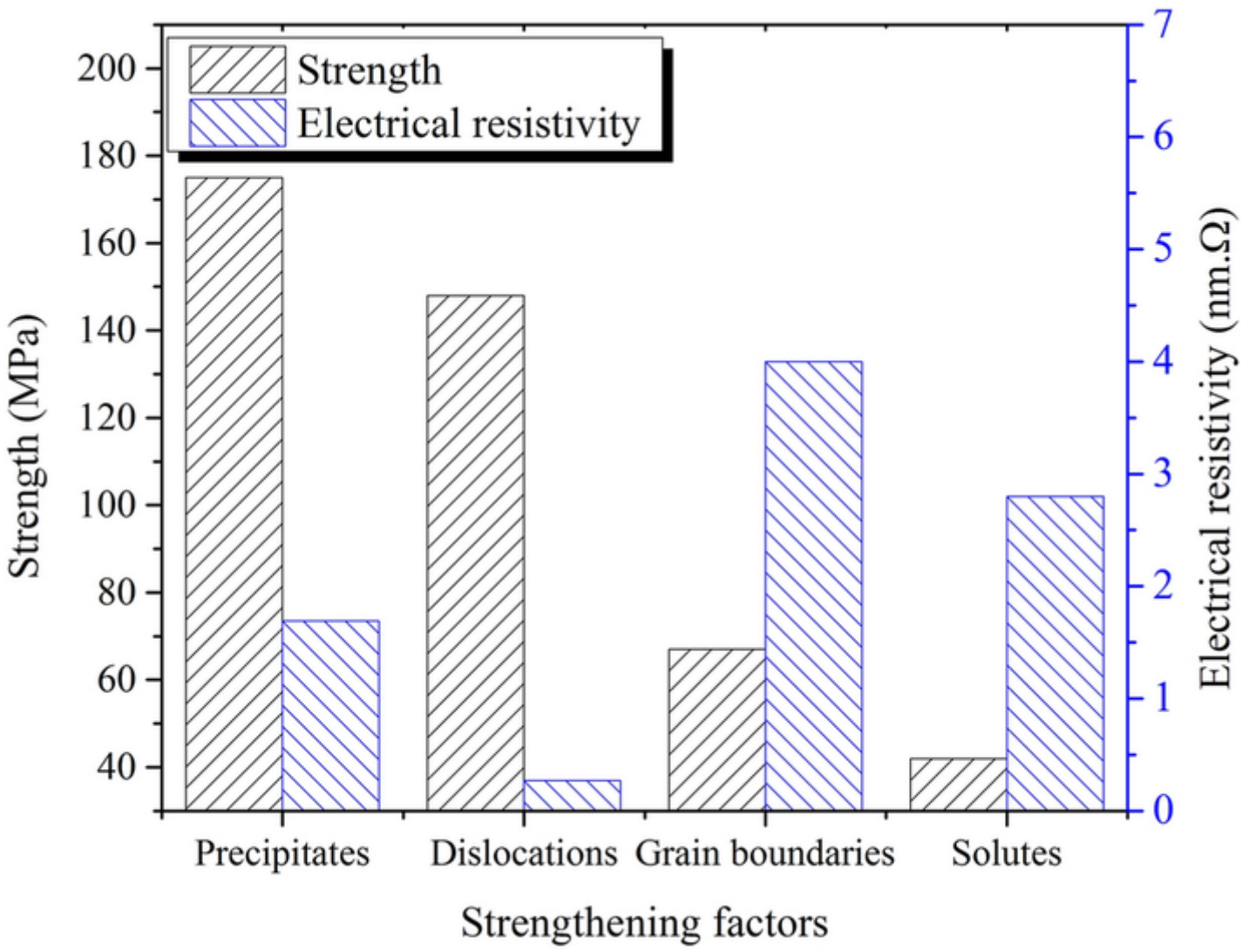

It is also supposed that the dislocation number density is 10^{15} m^{-2} and the Taylor factor is taken as 2. The contribution of dislocations to the strength using Eq. 6 and electrical resistivity using Eq. 12 is calculated to be 148 MPa and 0.27 nmΩ, respectively. It is meaningful that strain strengthening via dislocations is extremely effective on the strength increment with a low electrical resistivity, as displayed in Fig. 14. It is worthwhile to note that the strain hardening in the as-quenched state outperforms that in the peak-aged condition owing to the drag effect of the solutes on dislocations [37, 88]. Moreover, the dislocations could promote the extraction of alloying elements from the matrix to decrease electrical resistivity [30].

The average grain size of the sample is taken as 400 nm. The contribution of grain boundaries to the strength using Eq. 7 and electrical resistivity using Eq. 13 would be 67 MPa and 4 nmΩ, respectively. It shows a moderate impact of grain size on the strength even in the

case of ultrafine grains but with a considerable increase in electrical resistivity, as presented in Fig. 14. It is worth noting that grain boundary precipitates in ultrafine grains could decrease electrical resistivity but deteriorate the age-hardening response [25]. However, in the case of a normal grain size of 40 μm achievable by DC casting/extrusion or Properzi caster/hot rolling processes, the contribution of grain boundaries to the strength and electrical resistivity would be ~ 7 MPa and ~ 0.04 nmΩ, respectively, which are increasingly negligible. The grain size is inversely proportional to the electrical resistivity of grain boundaries based on Eq. 13.

For an AA6201 alloy containing 0.6% Mg and 0.6% Si, it is supposed that half of the solutes (0.3% Mg and 0.3% Si) remain in the matrix when the EC value meets the minimum required value. The contribution of Mg and Si solutes to the strength using Eq. 8 and electrical resistivity using Eq. 14 is estimated to be 42 MPa and 2.8 nmΩ, respectively.

The calculations obtained via the constitutive equations are displayed in Fig. 14. Accordingly, a relatively low level of solutes in the AA6201 alloy has the lowest strengthening impact among all strengthening factors with a remarkable increase in electrical resistivity. However, it has been reported that the impact of solute strengthening (especially Si) was experimentally beyond the value acquired via theoretical equations [26]. In contrast to solutes, precipitate hardening exhibited the highest strengthening effect with a relatively low electrical resistivity. The grain boundary with a nanograined structure has the most detrimental factor on electrical resistivity with a medium strengthening contribution. However, it has been reported that extensive grain boundaries lead to more purification of the matrix due to grain boundary precipitates and segregations. Finally, it is evident that strain hardening via dislocations possesses the second highest strengthening portion with negligible electrical resistivity [24].

Summary

Extensive attention has been given to Al–Mg–Si 6xxx conductor alloys in recent decades owing to their excellent mechanical properties, low mass resistivity, and low cost. As discussed in this review paper, there is a general trade-off between mechanical strength and electrical conductivity, which are mutually exclusive. To improve the electrical and mechanical properties, extensive research has been done based on the variations in the main alloying elements (Mg and Si), the addition of the other alloying elements, melt treatment, applying the modified thermomechanical treatments, and maximizing the area reduction (severe plastic deformation) in the wire drawing.

Excessive Si (Mg/Si~1) showed a better tensile strength with a desirable electrical conductivity in the coarse-grained 6xxx cables, while it exhibited superior electrical conductivity in the fine-grained 6xxx cables due to grain boundary precipitates and segregation. Some additional alloying elements (such as Sr) could boost the aging response and increase the tensile strength. Certain alloying elements (such as La and Ce) could improve electrical conductivity at the expense of strength since they were combined with Si to form new phases, depleting Si in the matrix.

The modified thermomechanical treatments led to a better combination of strength and electrical conductivity compared to conventional thermomechanical treatment. In addition, severe plastic deformation combined with aging could improve grain boundary strengthening and precipitate hardening with desirable electrical conductivity. Dynamic aging could prevent the formation of grain boundary precipitates.

A principal conclusion drawn in this review paper is that the strength should be enhanced by creating barriers (such as sessile dislocations and precipitates) for dislocation movement while having a less detrimental effect on the electrical conductivity. Experimental data and the strength and electrical resistivity models showed that precipitates and dislocations have promising effects on strength with minor negative electrical conductivity. Therefore, an M-TMT design ought to focus most on precipitate strengthening and dislocation hardening in Al–Mg–Si conductor alloys. In addition, grain boundary strengthening with nanoscale fine grains might be considered to improve the strength of Al–Mg–Si conductor alloys. Although the grain boundaries have a significant impact on the conductivity, they could indirectly lead to a less detrimental effect via grain boundary precipitates and segregation.

Future directions

Considering the potential to work on Al–Mg–Si conductor alloys based on the literature, the following directions have been outlined for future work.

1. The impact of intermediate aging on the significance of precipitate strengthening and strain hardening is not fully understood. Applying suitable intermediate aging could lead to high strength with a desirable electrical conductivity.
2. Applying M-TMT and the addition of effective alloying elements could be simultaneously taken into account. An appropriate M-TMT could maximize the efficiency of alloying elements on the precipitate strengthening with fewer solutes in the matrix.
3. A comprehensive study is required to elucidate the effect of microalloying elements, such as Sr, Bi, and Ag, on the electrical and mechanical properties of Al–Mg–Si 6xxx conductor alloys.

Acknowledgments

The authors would like to acknowledge the financial support of the Natural Sciences and Engineering Research Council of Canada (NSERC) under the Grant No. CRDPJ 514651-17 and Rio Tinto Aluminum through the Research Chair in the Metallurgy of Aluminum Transformation at University of Quebec in Chicoutimi.

Data availability

Data sharing is not applicable to this article as this is review article and that there were no new datasets generated or analyzed.

Declarations

Conflict of interest AQ2 On behalf of all authors, the corresponding author states that there is no conflict of interest.

Supplementary Information

Below is the link to the electronic supplementary material.

Supplementary file1 (DOCX 9531 kb)

References

1. L. Pan, K. Liu, F. Breton, X.G. Chen, Effect of Fe on microstructure and properties of 8xxx aluminum conductor alloys. J. Mater. Eng. Perform. **25**(12), 5201 (2016)

2. L. Pan, F.A. Mirza, K. Liu, X.G. Chen, Effect of Fe-rich particles and solutes on the creep behaviour of 8xxx alloys. Mater. Sci. Technol. **33**(9), 1130 (2016)

3. L. Pan, K. Liu, F. Breton, X.G. Chen, Effects of minor Cu and Mg additions on microstructure and material properties of 8xxx aluminum conductor alloys. J. Mater. Res. **32**(06), 1094 (2017)

4. R.B. Kalombo, J.M.G. Martínez, J.L.A. Ferreira, C.R.M. da Silva, J.A. Araujo, Comparative fatigue resistance of overhead conductors made of aluminium and aluminium alloy: tests and analysis. Procedia Eng. **133**, 223 (2015)

5. S. Karabay, Influence of AlB_2 compound on elimination of incoherent precipitation in artificial aging of wires drawn from redraw rod extruded from billets cast of alloy AA-6101 by vertical direct chill casting. Mater. Des. **29**(7), 1364 (2008)

6. S. Karabay, Modification of AA-6201 alloy for manufacturing of high conductivity and extra high conductivity wires with property of high tensile stress after artificial aging heat treatment for all-aluminium alloy conductors. Mater. Des. **27**(10), 821 (2006)

7. E. Cervantes, M. Guerrero, J.A. Ramos, S.A. Montes, Influence of natural aging and cold deformation on the mechanical and electrical properties of 6201–T81 aluminum alloy wires. Mater. Res. Soc. Symp. Proc. **3**, 14 (2010)

8. R.B. Kalombo, T.B. Miranda, P.H.C. Rocha, J.L.A. Ferreira, C.R.M. da Silva, J.A. Araujo, Fatigue performance of overhead conductors tested under the same value of H/w parameter. Procedia Eng. **213**, 346 (2018)

9. M. Iraizoz, N. Rossello, M. Amado, *Influence of Solution Heat Treatment Temperature in the Final Properties of AA6201 Drawn Wire, Light Metals 2015* (Springer International Publishing, Cham, 2016)

10. E. Rhaiem, T. Bouraoui and F. Elhalouani, Anticorrosive solution of 6201 aluminum alloy used in STEG company's overhead transmission lines, In: IOP Conference Series: Materials Science and Engineering, 13, 012038 (2010)

11. A. Laurino, E. Andrieu, J.-P. Harouard, J. Lacaze, M.-C. Lafont, G. Odemer, C. Blanc, Corrosion behavior of 6101 aluminum alloy strands for automotive wires. J. Electrochem. Soc. **160**(11), C569 (2013)

12. F.U. Flores, D.N. Seidman, D.C. Dunand, N.Q. Vo, Development of high-strength and high-electrical-conductivity aluminum alloys for power transmission conductors. Light Metals **247**, 15 (2018)

13. B. Smyrak, T. Knych, A. Mamala, K. Korzeń, P. Osuch, *A Study of the Influence of Strain Hardening and Precipitation Hardening Sequence on Mechanical Properties of AlMgSi Conductor Alloys* (Springer International Publishing, Cham, 2016)

14. Q. Zhao, Z. Qian, X. Cui, Y. Wu, X. Liu, Influences of Fe, Si and homogenization on electrical conductivity and mechanical properties of dilute Al–Mg–Si alloy. J Alloys Compd. **666**, 50 (2016)

15. Y. Han, D. Shao, B.A. Chen, Z. Peng, Z.X. Zhu, Q. Zhang, X. Chen, G. Liu, X.M. Li, Effect of Mg/Si ratio on the microstructure and hardness–conductivity relationship of ultrafine-grained Al–Mg–Si alloys. J. Mater. Sci. **52**(8), 4445 (2016)

16. R.Z. Valiev, M.Y. Murashkin, I. Sabirov, A nanostructural design to produce high-strength Al alloys with enhanced electrical conductivity. Scr. Mater. **76**, 13 (2014)

17. G.E. Totten, D.S. MacKenzie, *Handbook of Aluminum: Physical Metallurgy and Processes* (CRC Press, New York, 2003)

18. X. Sauvage, E.V. Bobruk, M.Y. Murashkin, Y. Nasedkina, N.A. Enikeev, R.Z. Valiev, Optimization of electrical conductivity and strength combination by structure design at the nanoscale in Al–Mg–Si alloys. Acta Mater. **98**, 355 (2015)

19. C.H. Liu, J. Chen, Y.X. Lai, D.H. Zhu, Y. Gu, J.H. Chen, Enhancing electrical conductivity and strength in Al alloys by modification of conventional thermo-mechanical process. Mater. Des. **87**, 1 (2015)

20. E. Standard: EN 50183. Conductors for overhead lines, aluminium magnesium silicon alloy wires, (2000)

21. ASTM, Annual Book of ASTM Standards: Electrical Conductors (2002)

22. ASTM: Annual Book of ASTM standards: nonferrous metal products. Aluminum and magnesium alloys. Section 2. Volume 02 (2003)

23. S. Karabay, E. Feyzullahoglu, Determination of early failure sources and mechanisms for Al 997% and Al–Mg–Si alloy bare conductors used in aerial transmission lines. Eng. Fail. Anal. **38**, 1 (2014)

24. X. Xu, Z. Yang, Y. Ye, G. Wang, X. He, Effects of various Mg/Si ratios on microstructure and performance property of Al-Mg-Si alloy cables. Mater. Charact. **119**, 114 (2016)

25. S. Jiang, R. Wang, Grain size-dependent Mg/Si ratio effect on the microstructure and mechanical/electrical properties of Al-Mg-Si-Sc alloys. J. Mater. Sci. Technol. **35**(7), 1354 (2019)

26. S.N. Khangholi, M. Javidani, A. Maltais, X.G. Chen, Optimization of mechanical properties and electrical conductivity in Al–Mg–Si 6201 alloys with different Mg/Si ratios. J Mater Res. **35**(20), 2765 (2020)

27. S.N. Khangholi, M. Javidani, A. Maltais, X.G. Chen, Investigation on electrical conductivity and hardness of 6xxx aluminum conductor alloys with different Si levels. MATEC Web Conf. **326**, 1 (2020)

28. M.H. Mulazimoglu, A. Zaluska, F. Paray, J.E. Gruzleski, The effect of strontium on the Mg2Si precipitation process in 6201 aluminum alloy. Metall. Mater. Trans. A. **28**(6), 1289 (1997)

29. X. Cui, Y. Wu, G. Zhang, Y. Liu, X. Liu, Study on the improvement of electrical conductivity and mechanical properties of low alloying electrical aluminum alloys. Compos. B. Eng. **110**, 381 (2017)

30. G. Lin, Z. Zhang, H. Wang, K. Zhou, Y. Wei, Enhanced strength and electrical conductivity of Al–Mg–Si alloy by thermo-mechanical treatment. Mater. Sci. Eng. A. **650**, 210 (2016)

31. C. Bunte, M. Glassel, C. Medina, D. Zalcman, Proposed solution for random characteristics of aluminium alloy wire rods due to the natural aging. Procedia Mater. Sci. **9**, 97 (2015)

32. J.P. Hou, Q. Wang, Z.J. Zhang, Y.Z. Tian, X.M. Wu, H.J. Yang, X.W. Li, Z.F. Zhang, Nano-scale precipitates: the key to high strength and high conductivity in Al alloy wire. Mater. Des. **132**, 148 (2017)

33. K. Majchrowicz, Z. Pakieła, W. Chrominski, M. Kulczyk, Enhanced strength and electrical conductivity of ultrafine-grained Al-Mg-Si alloy processed by hydrostatic extrusion. Mater Charact. **135**, 104 (2018)

34. M.Y. Murashkin, I. Sabirov, V.U. Kazykhanov, E.V. Bobruk, A.A. Dubravina, R.Z. Valiev, Enhanced mechanical properties and electrical conductivity in ultrafine-grained Al alloy processed via ECAP-PC. J. Mater. Sci. **48**(13), 4501 (2013)

35. M. Murashkin, A. Medvedev, V. Kazykhanov, A. Krokhin, G. Raab, N. Enikeev, R. Valiev, Enhanced Mechanical Properties and Electrical Conductivity in Ultrafine-Grained Al 6101 Alloy Processed via ECAP-Conform. Metals. **5**(4), 2148 (2015)

36. X. Ji, H. Zhang, S. Luo, F. Jiang, D. Fu, Microstructures and properties of Al–Mg–SI alloy overhead conductor by horizontal continuous casting and continuous extrusion forming process. Mater. Sci. Eng. A. **649**, 128 (2016)

37. S.N. Khangholi, M. Javidani, A. Maltais, X.G. Chen, Effects of natural aging and pre-aging on the strength and electrical conductivity in Al-Mg-Si AA6201 conductor alloys. Mater. Sci. Eng. A. **820**, 1 (2021)

38. D. Lindholm, S. Akhtar, D. Mortensen, Numerical simulation of wire rod casting of AA1370 and AA6101 alloys. Light Metals **50**, 1032 (2020)

39. R.M. Mustafa, Production of aluminium-silicon-magnesium wrought alloy rod with application in the manufacture of extra-high conductivity AAAC for overhead electrical transmission lines. Light Metals **613**, 15 (2008)

40. ASM Handbook: Casting, Volume 15. ASM International (1998)

41. T.G. Zhou, Z.Y. Jiang, J.L. Wen, H. Li, A.K. Tieu, Semi-solid continuous casting–extrusion of AA6201 feed rods. Mater. Sci. Eng. A **485**(1–2), 108 (2008)

42. G.A. Edwards, K. Stiller, G.L. Dunlop, M.J. Couper, The precipitation sequence in Al–Mg–Si alloys. Acta Mater. **46**(11), 3893 (1998)

43. J. Buha, R.N. Lumley, A.G. Crosky, K. Hono, Secondary precipitation in an Al–Mg–Si–Cu alloy. Acta Mater. **55**(9), 3015 (2007)

44. S.J. Andersen, H.W. Zandbergen, J. Jansen, C. Traeholt, U. Tundal, O. Reiso, The crystal structure of the β″ phase in Al–Mg–Si alloys. Acta Mater. **3283**, 3283–3298 (1998)

45. K. Teichmann, C.D. Marioara, S.J. Andersen, K.O. Pedersen, S. Gulbrandsen-Dahl, M. Kolar, R. Holmestad, K. Marthinsen, HRTEM study of the effect of deformation on the early precipitation behaviour in an AA6060 Al–Mg–Si alloy. Philos. Mag. **91**(28), 3744 (2011)

46. R.S. Yassar, D.P. Field, H. Weiland, The effect of predeformation on the β″ and β′ precipitates and the role of Q′ phase in an Al–Mg–Si alloy; AA6022. Scr. Mater. **53**(3), 299 (2005)

47. H. Nemour, D.M. Ibrahim, A. Triki, The effect of heavy cold plastic deformation on the non-isothermal kinetics and the precipitation sequence of metastable phases in an Al–Mg–Si alloy. J. Therm. Anal. Calorim. **123**(1), 19 (2015)

48. G. Sha, H. Moller, W.E. Stumpf, J.H. Xia, G. Govender, S.P. Ringer, Solute nanotructures and their strengthening effects in Al–7Si–06Mg alloy F357. Acta Mater. **60**(2), 692 (2012)

49. J.H. Chen, E. Costan, M.A. van Huis, Q. Xu, H.W. Zandbergen, Atomic pillar-based nanoprecipitates strengthen AlMgSi alloys. Science **312**(5772), 416 (2006)

50. H.S. Hasting, A.G. Froseth, S.J. Andersen, R. Vissers, J.C. Walmsley, C.D. Marioara, F. Danoix, W. Lefebvre, R. Holmestad, Composition of β″ precipitates in Al–Mg–Si alloys by atom probe tomography and first principles calculations. J. Appl. Phys. **106**(12), 123527 (2009)

51. H.W. Zandbergen, S.J. Andersen, J. Jansen, Structure determination of Mg_5Si_6 particles in Al by dynamic electron diffraction studies. Science **277**, 1221 (1997)

52. ASM Handbook: Properties and Selections Nonferrous Alloys and Special-Purpose Materials, 507 (1990)

53. A.K. Gupta, D.J. Lloyd, S.A. Court, Precipitation hardening in Al–Mg–Si alloys with and without excess Si. Mater. Sci. Eng. A **316**(1), 11 (2001)

54. Y. Weng, Z. Jia, L. Ding, Y. Pan, Y. Liu, Q. Liu, Effect of Ag and Cu additions on natural aging and precipitation hardening behavior in Al-Mg-Si alloys. J Alloys Compd. **695**, 2444 (2017)

55. C.D. Marioara, S.J. Andersen, H.W. Zandbergen, R. Holmestad, The influence of alloy composition on precipitates of the Al-Mg-Si system. Metall. Mater. Trans. A **36**(3), 691 (2005)

56. C.D. Marioara, S.J. Andersen, T.N. Stene, H. Hasting, J. Walmsley, A.T.J. Van Helvoort, R. Holmestad, The effect of Cu on precipitation in Al–Mg–Si alloys. Philos. Mag. **87**(23), 3385 (2007)

57. K. Li, A. Beche, M. Song, G. Sha, X. Lu, K. Zhang, Y. Du, S.P. Ringer, D. Schryvers, Atomistic structure of Cu-containing β ″precipitates in an Al–Mg–Si–Cu alloy. Scr. Mater. **75**, 86 (2014)

58. M. Murayama, K. Hono, Pre-precipitate clusters and precipitation processes in Al–Mg–Si alloys. Acta Mater. **47**(5), 1537 (1999)

59. L. Ding, Z. Jia, Y. Liu, Y. Weng, Q. Liu, The influence of Cu addition and pre-straining on the natural aging and bake hardening response of Al-Mg-Si alloys. J Alloys Compd. **688**, 362 (2016)

60. L.-X. Cui, Z.-X. Liu, X.-G. Zhao, J.-G. Tang, K. Liu, X.-X. Liu, C. Qian, Precipitation of metastable phases and its effect on electrical resistivity of Al-096Mg2Si alloy during aging. Nonferr Metal. Soc. **24**(7), 2266 (2014)

61. B. Smyrak, B. Jurkiewicz, M. Zasadzinska, M. Gniełczyk, P. Jałowy, The effect of Al-Mg-Si wire rod heat treatment on its electrical conductivity and strength. Metals. **10**(8), 1027 (2020)

62. W. Yuan, Z. Liang, Effect of Zr addition on properties of Al–Mg–Si aluminum alloy used for all aluminum alloy conductor. Mater. Des. **32**(8–9), 4195 (2011)

63. T. Ikeda, T. Muto, K. Morimoto, Effects of zirconium addition and solute iron concentration on the softening behavior of 6101 aluminum conductor alloy. Mater Sci Forum. **331–337**, 595 (2000)

64. W. Yuan, Z. Liang, C. Zhang, L. Wei, Effects of La addition on the mechanical properties and thermal-resistant properties of Al–Mg–Si–Zr alloys based on AA 6201. Mater. Des. **34**, 788 (2012)

65. M. Hosseinifar, D.V. Malakhov, The sequence of intermetallics formation during the solidification of an Al-Mg-Si Alloy containing La. Metall. Mater. Trans. A **42**(3), 825 (2010)

66. M.H. Mulazimoglu, A. Zaluska, J.E. Gruzleski, F. Paray, Electron microscope study of Al-Fe-Si intermetallics in 6201 aluminum alloy. Metall. Mater. Trans. A **27**(4), 929 (1996)

67. H.C. Liao, Y. Liu, C.L. Lu, Q.G. Wang, Effect of Ce addition on castability, mechanical properties and electric conductivity of Al–03Si–02Mg alloy. Int. J. Cast. Met. Res. **28**(4), 213 (2015)

68. D.G. Eskin, *Physical Metallurgy of Direct Chill Casting of Aluminum Alloys* (Taylor & Francis, New York, 2008)

69. S. Wang, K. Matsuda, T. Kawabata, Y. Zou, T. Yamazaki, S. Ikeno, Effect of TM-addition on the aging behaviour of Al-Mg-Si alloys. Mater. Trans. **52**(2), 229 (2011)

70. L. Backerud, E. Krol and J. Tamminen: solidification characteristics of aluminum alloys: wrought alloys (1986).

71. Y. Weng, Z. Jia, L. Ding, S. Muraishi, Q. Liu, Clustering behavior during natural aging and artificial aging in Al-Mg-Si alloys with different Ag and Cu addition. Mater. Sci. Eng. A **732**, 273 (2018)

72. T. Saito, E.A. Mortsell, S. Wenner, C.D. Marioara, S.J. Andersen, J. Friis, K. Matsuda, R. Holmestad, Atomic structures of precipitates in Al-Mg-Si alloys with small additions of other elements. Adv. Eng. Mater. **20**(7), 24 (2018)

73. S. Karabay, E.A. Guven, A.T. Erturk, Enhancement on Al–Mg–Si alloys against failure due to lightning arc occurred in energy transmission lines. Eng. Fail. Anal. **31**, 153 (2013)

74. X. Cui, Y. Wu, X. Liu, Q. Zhao, G. Zhang, Effects of grain refinement and boron treatment on electrical conductivity and mechanical properties of AA1070 aluminum. Mater. Des. **86**, 397 (2015)

75. M. Kolar, K.O. Pedersen, S. Gulbrandsen-Dahl, K. Marthinsen, Combined effect of deformation and artificial aging on mechanical properties of Al–Mg–Si Alloy. Nonferr Metal Soc. **22**(8), 1824 (2012)

76. M. Kolar, K.O. Pedersen, S. Gulbrandsen-Dahl, K. Teichmann, K. Marthinsen, Effect of pre-deformation on mechanical response of an artificially aged Al-Mg-Si Alloy. Mater. Trans. **52**(7), 1356 (2011)

77. M. Li, H. Li, Z. Zhang, W. Shi, J. Liu, Y. Hu, Y. Wu, Effect of precipitates on properties of cold-rolled Al–Mg–Si–Sc–Zr alloy with higher temperature aging. Mater. Sci. Technol. **34**(10), 1246 (2018)

78. Z.H. Zhao, Q.Q. Chen, Q.F. Zhu, W.Q. Liu, G.S. Wang, Study on the ageing process of the 6xxx series aluminum alloy wires for overhead conductors. Mater Sci Forum. **877**, 347 (2016)

79. P.A. Rometsch, Z. Xu, H. Zhong, H. Yang, L. Ju, X.H. Wu, Strength and electrical conductivity relationships in Al-Mg-Si and Al-Sc alloys. Mater Sci Forum. **794–796**, 827 (2014)

80. Y. Aruga, S. Kim, M. Kozuka, E. Kobayashi, T. Sato, Effects of cluster characteristics on two-step aging behavior in Al-Mg-Si alloys with different Mg/Si ratios and natural aging periods. Mater. Sci. Eng. A **718**, 371 (2018)

81. G.H. Tao, C.H. Liu, J.H. Chen, Y.X. Lai, P.P. Ma, L.M. Liu, The influence of Mg/Si ratio on the negative natural aging effect in Al–Mg–Si–Cu alloys. Mater. Sci. Eng. A **642**, 241 (2015)

82. M.C. Lentz, M. Rengel, K. Stray, O. Engler, A modified processing route for high strength Al-Mg-Si aluminum conductors based on twin-roll cast strip. J. Mater. Process. Technol. **278**, 116463 (2020)

83. Z.P. Martinova: Pre-aging effects in thermo mechanically treated 6201 aluminium alloy Macedonian Union of Metallurgists, Skopje Macedonian Union of Metallurgists, 161 (2003)

84. H. Li, M. Qingzhong, Z. Wang, F. Miao, B. Fang, R. Song, Z. Zheng, Simultaneously enhancing the tensile properties and intergranular corrosion resistance of Al–Mg–Si–Cu alloys by a thermo-mechanical treatment. Mater. Sci. Eng. A. **617**, 165 (2014)

85. Z. Wang, H. Li, F. Miao, B. Fang, R. Song, Z. Zheng, Improving the strength and ductility of Al–Mg–Si–Cu alloys by a novel thermo-mechanical treatment. Mater. Sci. Eng. A **607**, 313 (2014)

86. X. Sauvage, M.Y. Murashkin, R.Z. Valiev, Atomic scale investigation of dynamic precipitation and grain boundary segregation in a 6061 aluminium alloy nanostructured by ECAP. Kovove Mater. **49**, 11 (2011)

87. M. Murayama, Z. Horita, K. Hono, Microstructure of two-phase Al–17 at% Cu alloy deformed by equal-channel angular pressing. Acta Mater. **49**(1), 21 (2001)

88. L.M. Cheng, W.J. Poole, J.D. Embury, D.J. Lloyd, The influence of precipitation on the work-hardening behavior of the aluminum alloys AA6111 and AA7030. Metall Mater. Trans. A **34**(11), 2473 (2003)

89. J.K. Sunde, C.D. Marioara, S. Wenner, R. Holmestad, On the microstructural origins of improvements in conductivity by heavy deformation and ageing of Al-Mg-Si alloy 6101. Mater. Charact. **176**, 1 (2021)

90. W. Yuna, Z. Jianfeng, L. Hengcheng, W. Yongjin, W. Yuping, Effect of homogenization temperature on microstructure and conductivity of Al-Mg-Si-Ce alloy. J. Mater. Eng. Perform. **25**(7), 2720 (2016)

91. S. Karabay, M. Yilmaz, M. Zeren, Investigation of extrusion ratio effect on mechanical behaviour of extruded alloy AA-6101 from the billets homogenised-rapid quenched and as-cast conditions. J. Mater. Process. Technol. **160**(2), 138 (2005)

92. H. Liao, Y. Wu, Y. Wang, Microstructure Evolution of Al-035%Si-02%Mg-03%Ce Alloy During Hot Extrusion and Its Contributions to Performances. J. Mater. Eng. Perform. **24**(6), 2503 (2015)

93. M. Javidani, D. Larouche, Application of cast Al–Si alloys in internal combustion engine components. Int. Mater. Rev. **59**(3), 132 (2014)

94. Y. Wu, H. Liao, J. Zhang, Effect of intermediate annealing temperature and aging on the mechanical properties and conductivity of Al–02Mg–035Si–03Ce wire rod. High Perform. Struct. Mater. **139**, 40 (2018)

95. J. Zhang, M. Ma, F. Shen, D. Yi, B. Wang, Influence of deformation and annealing on electrical conductivity, mechanical properties and texture of Al-Mg-Si alloy cables. Mater. Sci. Eng. A **710**, 27 (2018)

96. P. Osuch, M. Walkowicz, T. Knych, S. Dymek, Impact of the direct ageing procedure on the age hardening response of Al-Mg-Si 6101 alloy. Materials (Basel). **11**(7), 1239 (2018)

97. V.D. Sitdikov, M.Y. Murashkin and R.Z. Valiev: Precipitates studies in ultrafine-grained Al alloys with enhanced strength and conductivity. *IOP Conference Series: Materials Science and Engineering*. **194**, (2017)

98. M.Y. Murashkin, I. Sabirov, X. Sauvage, R.Z. Valiev, Nanostructured Al and Cu alloys with superior strength and electrical conductivity. J. Mater. Sci. **51**(1), 33 (2015)

99. A. Medvedev, M.Y. Murashkin, V. Kazykhanov, R.Z. Valiev, A.E. Medvedev, P.D. Hodgson, R. Lapovok, Enhancement of mechanical and electrical properties in Al 6101 alloy by severe shear strain under hydrostatic pressure. Adv Eng Mater. **20**(11), 1800695 (2018)

100. O. Engler, C.D. Marioara, Y. Aruga, M. Kozuka, O.R. Myhr, Effect of natural ageing or pre-ageing on the evolution of precipitate structure and strength during age hardening of Al–Mg–Si alloy AA 6016. Mater. Sci. Eng. A **759**, 520 (2019)

101. T. Khelfa, M.A. Rekik, J.A. Munoz-Bolanos, J.M. Cabrera-Marrero, M. Khitouni, Microstructure and strengthening mechanisms in an Al-Mg-Si alloy processed by equal channel angular pressing (ECAP). Int. J. Adv. Manuf. Technol. **95**(1–4), 1165 (2017)

102. Y.J. Li, A.M.F. Muggerud, A. Olsen, T. Furu, Precipitation of partially coherent α-Al(Mn, Fe)Si dispersoids and their strengthening effect in AA 3003 alloy. Acta Mater. **60**(3), 1004 (2012)

103. Z. Li, Z. Zhang, X.G. Chen, Improvement in the mechanical properties and creep resistance of Al-Mn-Mg 3004 alloy with Sc and Zr addition. Mater. Sci. Eng. A **729**, 196 (2018)

104. W. Wen, Y. Zhao, J.G. Morris, The effect of Mg precipitation on the mechanical properties of 5xxx aluminum alloys. Mater. Sci. Eng. A **392**(1–2), 136 (2005)

105. B. Raeisinia, W.J. Poole, D.J. Lloyd, Examination of precipitation in the aluminum alloy AA6111 using electrical resistivity measurements. Mater. Sci. Eng. A **420**(1), 245 (2006)